

Proposal for a Full-Scale Detector Engineering Test and Test Beam Calibration of a Single-Phase LAr TPC

A. name¹, B. name², and C. name³

¹Department of X1, University Y1

²Department of X2, University Y2

³Department of X3, University YY3

February 18, 2015

Abstract

insert abstract here

Contents

| | | |
|----------|--|-----------|
| 1 | Introduction [~5 pages; Thomas/Greg/Bob Wilson] | 3 |
| 1.1 | Physics goals of LBNF | 3 |
| 1.2 | Single-phase LAr TPC Prototype | 3 |
| 1.3 | Goals for the prototype run | 4 |
| 2 | CERN prototype detector and charged particle beam test [~10 pages; Donna/Jarek] | 4 |
| 2.1 | Requirements for the detector, beam and commissioning | 4 |
| 2.2 | Detector performance tests | 8 |
| 2.3 | Other measurements | 10 |
| 3 | Single Phase LAr Detector [~10 pages; J. Stewart et al.] | 10 |
| 3.1 | LBNF detector | 10 |
| 3.2 | CERN prototype detector | 12 |
| 4 | Photon Detector | 28 |
| 4.1 | Introduction | 28 |
| 4.2 | Baseline Design (TPB-Coated Acrylic Bars) | 28 |
| 4.3 | Alternate 1: Coated Acrylic Plate with Fiber Readout | 29 |
| 4.4 | Alternate 2: Fiber Bundle with TPB-coated radiator | 29 |
| 4.5 | Technology Selection | 29 |
| 5 | Cryostat and cryogenics system [~5 pages; David/Barry/Jack] | 34 |
| 5.1 | LBNF detector | 34 |
| 5.2 | CERN prototype detector | 34 |
| 5.3 | Cryogenic System (from David Montanari) | 44 |
| 6 | Charged Particle Test Beam Requirements [~10 pages; Cheng-Ju] | 47 |
| 6.1 | Particle Beam Requirements | 47 |
| 6.2 | EHN1 H4ext Beamline | 48 |
| 6.3 | Beam Instrumentation | 49 |
| 6.4 | Muon Beam Halo Counters | 49 |
| 6.5 | Beam Window on LAr Cryostat | 49 |
| 7 | Computing requirements, data handling and software [~3 pages; Maxim Potekhin/Craig Tull] | 49 |
| 7.1 | Overview | 49 |
| 7.2 | Collecting and Storing Raw Data | 50 |
| 7.3 | Databases | 53 |
| 7.4 | A note on Simulation and Reconstruction Software | 54 |
| 7.5 | Distributed Computing, Workload and Workflow Management | 54 |

1 Introduction [~5 pages; Thomas/Greg/Bob Wilson]

This document is a technical report for the Expression of Interest <reference> submitted to the CERN SPSC in October 2014. In this report, we detail the proposal to test full-scale detector elements for a single-phase liquid argon (LAr) TPC based on the former LBNE design which is a potential viable technology for use as a far detector for the experiment that will be at the Long Baseline Neutrino Facility (LBNF). To mitigate the risks associated with extrapolating small scale versions of the single-phase LAr TPC technology to a full-scale detector element, it is essential to benchmark the operation of a full-scale detector elements in a particle beam. The beam facility at the CERN Neutrino Platform (cite) provides an opportunity to perform this crucial test of the proposed single-phase LAr TPC and inform the decision regarding phased implementation of the far detector for LBNF.

1.1 Physics goals of LBNF

An international collaboration is forming that will utilize a proposed 1.2 MW proton beam at FNAL to create a neutrino beam that will be directed at the Homestake Mine in the USA. The proposal is to place by the year 2024 <mention 2021 date for 10kton> a 40 kton LAr TPC in the underground facility at Homestake to observe the oscillation of $\nu_\mu \rightarrow \nu_e$ and $\bar{\nu}_\mu \rightarrow \bar{\nu}_e$ that occur near a neutrino energy of 3 GeV and thereby make precision measurements of δ_{CP} , δ_{13} , and δ_{23} and determining the neutrino mass hierarchy. In order to make such precise measurements, the detector will need to accurately identify and measure the energy of the particles produced in the neutrino interaction with Argon which will range from a few GeV to hundreds of MeV.

1.2 Single-phase LAr TPC Prototype

The LBNE-style single-phase LAr TPC is design to be scalable using module units that consist of a factory-built anode plane, a cathode a plane, and a field cage with the anode plane assemblies measuring 6.0m (h) \times 2.3m (w) \times 0.09m (d) and a drift length of 2.5m. The electronics will be mounted in the cryostat on the wire planes to reduce the number of cables that penetrate the cryostat and optimize the electronic signal to noise. Event timing will be determined through the use of scintillation photon detectors that will use light collection paddles. With this modular design as shown in <insert figure of LBNE detector to shown modular design>, it will be possible to achieve the goal of 40 kton detector for the LBNF far site.

Some features of this single-phase design will be tested using smaller scale prototypes such as the ongoing tests with a 35ton unit at Fermilab and the 5ton CAPTAIN LAr TPC. However, none of these smaller prototypes uses full scale detector elements or are large enough to fully contain particles. Considering that the detector at the LBNF far site will be about a factor of 50 larger in scale than the ICARUS detector which is currently the largest LAr TPC detector built to date, it is essential to validate the full-scale detector elements in a particle beam at the CERN Neutrino Platform.

In order to fully contain particles within the energy range of interest and provide space for detector services, the cryostat will need to have a minimum inner dimensions of 8.4m (h) \times 7.3m (w) \times 9.5m (d). It is anticipated that the CERN Neutrino Platform will facilitate the design and construction of the cryostat and that this effort will common area that will motivate collaboration with the WA105 team.

1.3 Goals for the prototype run

The goals of the prototype run include:

- Use of particle beam to assess
 - tracking and calorimetric response
 - reconstruction algorithm
 - Monte Carlo simulation
 - Secondary hadron interactions in detector
- Verifying argon contamination mitigation
- Full-scale structural test under LAr cryogenic conditions
- Verification of TPC Electrics under LAr cryogenic conditions
- Study light levels of the photon detection system
- Developing installation procedures for full-scale electronics

2 CERN prototype detector and charged particle beam test [\sim 10 pages; **Donna/Jarek**]

describe and motivate proposed detector and beam test requirements

2.1 Requirements for the detector, beam and commissioning

The Single-Phase Cern Prototype detector is intended to provide necessary information to reduce systematic uncertainties for the oscillation measurements in the US-based long base-line neutrino experiment. The LAr TPC technology is not new but wasn't extensively used in the 1-10 GeV neutrino energy range. The main source of uncertainties due to detector with the current values are shown in table 1

With current detector uncertainties from table 1 the sensitivities for the CP violation phase measurement is shown in Fig. 2.1 **Task: make this plot**. The proposed test beam detector will reduce uncertainties to XX% and improve our sensitivity to δ_{CP} as shown in Fig. 2.1 **Task: make this plot**.

Table 1: Current known sources of detector uncertainties for liquid argon or TPC.

| source of uncertainty | value | reference |
|---|-------|-----------|
| e/ γ separation | | |
| e-m shower calibration | | |
| hadronic shower calibration | | |
| low energy acceptance electron identification | | |
| | | |

Table 2: Current known sources of uncertainties due to interaction of charged particle with argon.

| source of uncertainty | value | reference |
|--|-------|-----------------------|
| pion(Kaon) absorbtion | | |
| pion(Kaon) charge exchange | | |
| pion (Kaon) production in secondary interactions | | |
| muon capture | | Phys. Rev. C 35, 2212 |
| energy scale | | |
| Michel electron tagging | | |
| | | |

Figure 1: Sensitivities for the δ_{CP} measurement for using current knowledge of the single-phase LAr-TPC detector technology and for reduced detector uncertainties from SPCP beamtest data. The plots prepared for 40 kton fiducial mass and $xx \times 10^{21}$ POT.

2.1.1 Particles energy and direction

Plans for running beam for the the ELBNF include both neutrino and anti-neutrino configurations. These beams will be composed mainly of muon neutrinos (anti-neutrinos) as well as electron neutrinos (anti-neutrinos). In figures 2.1.1 and 2.1.1 the distributions on momenta and angles of particles created in neutrino interaction are shown.

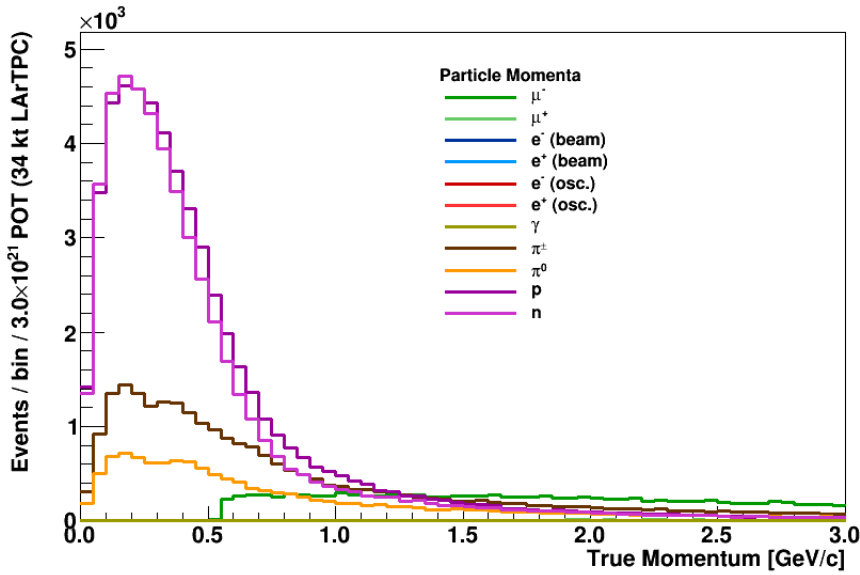


Figure 2: Particle momenta distributions for particles coming from all fluxes (ν_e , ν_μ , $\bar{\nu}_e$ and $\bar{\nu}_\mu$) at both near and far detector locations.

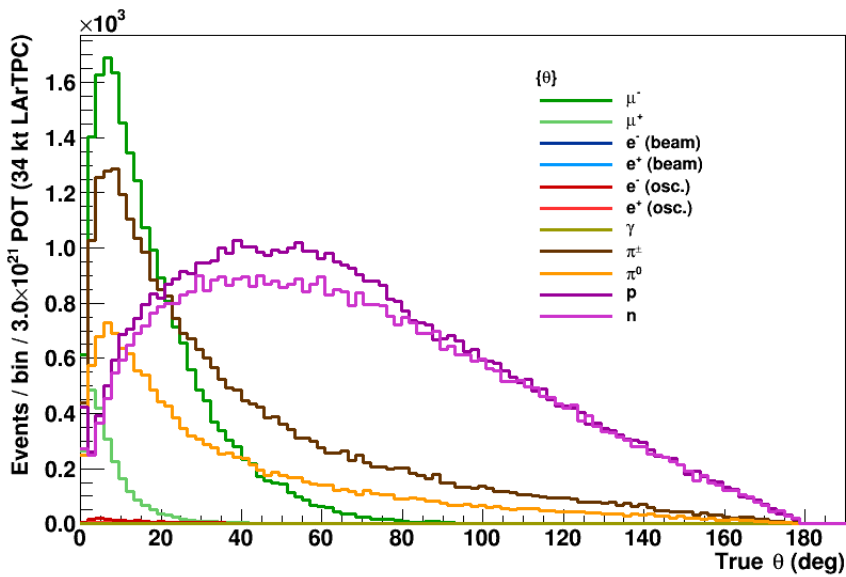


Figure 3: Particle angle wrt to the beam axis distributions for particles coming from all fluxes (ν_e , ν_μ , $\bar{\nu}_e$ and $\bar{\nu}_\mu$) at both near and far detector locations.

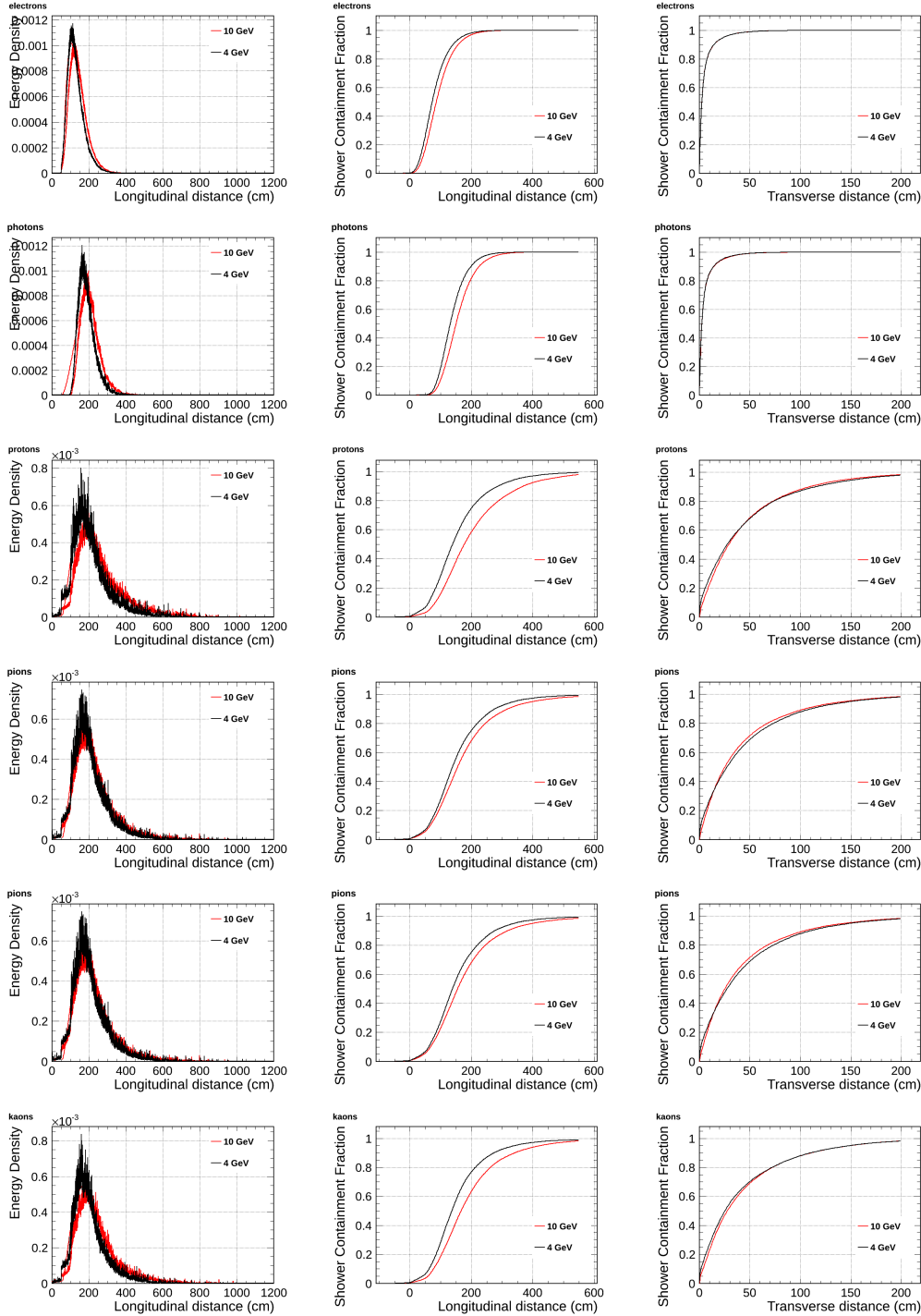


Figure 4: Particle containment plots.

2.1.2 Particle rates

Estimation of beam particles rates necessary to collect high enough statistics in a reasonable time to obtain goals of the measurements.

2.1.3 Run plan

Based of the rates from the beam and required rates from the physics considerations.

2.2 Detector performance tests

2.2.1 Bethe-Bloch parametrisation of charged particles

The SPCP will allow to study the detector response to charge particles from the test beam and will serve as a calibration detector. The measured energy deposition for various particles and its dependence on the direction of the particle will feed into our Monte Carlo generator and allow more precise reconstruction of neutrino energy and interactions topologies with good particle identifications.

How we compare with Lariat? Multiple scattering

The set of single-phase prototype detector helped to understand the detector response to cosmic muons. But there is still lots to learn with additional studies. The charge particle identification efficiencies has been mapped for only limited range of the particle energies.

2.2.2 e/ γ separation

The separation of the electrons from photons is the most important feature of the LAr TPC detectors for the search of the CP violation phase where we look for appearance of the ν_e in the ν_μ beam. Showers from electrons are part of the signal whilst the single photons might contribute to the background sample. The photons can undergo two process: pair production and Compton scattering. The dominant process for photons with energies of several hundreds MeV is the $e^+ e^-$ pair production, but Compton scattering also occur at this energies. For pair production the e/ γ separation is achieved by looking at the beginning of the electromagnetic shower, where for election we see energy deposition typical for single MIP and for photon we see energy deposition consisted with two MIP. The separation of e/ γ has been measured in the ArgoNEUT experiment using neutrino scattering data with low statistics. Currently the separation efficiency is estimated to be at the level of 94 % (? cite and check the number). In case of the Compton scattering the off atomic electron the signal is much more difficult to distinguish from the electron from the CC ν_e scattering.

The separation of the e/ γ measured by ArgoNEUT is not sufficient for the ELBNF experiment. Here we propose a measurement of the separation

efficiency as the function of energy and angle. we need someone to look into this

2.2.3 Reconstruction efficiencies and particle identification

The reconstruction of events in the LAr TPC is still a challenge but rapid progress has been achieved in recent years (cite pandora and other reconstruction algorithms). Despite the progress reconstruction algorithms have to rely Monte Carlo predictions which don't simulate liquid argon detectors responses correctly. Reconstruction algorithms will benefit greatly from test beam data particularly from the full scale prototype. The reconstruction algorithms will be trained to correctly reconstruct track, electromagnetic and hadronic showers.

The data of tracks and showers can be used to create a library which can be used for matching with he neutrino data, similar to the LEM (library event matching).

Main issues for the reconstruction algorithms:

- The reconstruction algorithms try to use all three planes on the signal readout. if the orientation of the track/shower is such that it is aligned with wires on one of the plans it significantly reduces quality of reconstructed objects.
- Calorimetry with collection and induction planes. In the ICARUS experiment the deposited energy was reconstructed from the signal on the collection plane. The induction planes bipolar signal wasn't "stable" enough to use it for calorimetric measurement. In the ELBNF design there is additional shielding wire plane which will improve the quality of the bipolar signal and the test beam experiment will help with its calibration.
- Vertexing.
- Reconstruction efficiency for low energy particles. The reconstruction algorithm suffer from the lose of fefficiency for low energy particle or particles which leave less than 200-300 hits. Training the algorithms on a low energy particles from the test beam will improve the quality and efficiency of the reconstructed objects.

2.2.4 Cross section measurements

Precise measurement of the absorption and charge exchange of pions and kaons. Pion absorption is a large part of the pion nucleon cross section from 50 MeV to 500MeV with no data above about 1GeV pion kinetic energy. Add plots and values for known cross sections wit errors

- pion absorption on argon - Kotlinski, EPJ 9, 537 (2000)
- pion cross section as a function of A - Gianelli PRC 61, 054615 (2000)

There is not currently a satisfactory theory describing absorption. The Valencia group (Vicente-Vacus NPA 568, 855 (1994)) developed model of the pion-nucleus reaction with fairly good agreement, although not in detail. The actual mechanism of multi-nucleon absorption is not well understood.

2.2.5 Charge sign determination

It is not possible to determine charge of the particle on the event by event basis with non-magnetised LAr TPC detectors. However, the statistical analyst will be possible. We will fit the muon's half time which is different for muons and antimony due to different muon capture cross sections. For the μ^+ for argon we expect about xx% to be captured and for μ^- about yy%.

2.2.6 Single track calibration

2.2.7 Shower calibration

Reconstruction of neutrino energy depends of a quality of reconstruction of both electromagnetic and hadronic showers.

- features of Hadronic shower in LAr TPC - features of electromagnetic shower in LAr TPC - Missing energy from neutral (Neutrons scattering)

2.3 Other measurements

2.3.1 Anti-proton annihilation

2.3.2 Proton decay background (cosmogenic $K^0 \rightarrow K^+$)

3 Single Phase LAr Detector [\sim 10 pages; **J. Stewart et al.**]

3.1 LBNF detector

The far detector for the ELBNF collaboration will be a series of four xx kt (10 kt) active (fiducial) volume liquid argon time projection chambers instrumented with photon detection. It is planned that the first 10 kt detector will be ready for commissioning in 2021. One option for the TPC design is a wire plane based TPC with cold electronics readout. Designs of this style are referred to as single-phase detectors as the charge generation, drift, and detection all occurs in the argon liquid phase. This style TPC has the advantage that there is no charge amplification before collection making a very precise charge measurement possible. To achieve ELBNF's goals, a detector much larger than ICARUS, the largest LAr TPC detector built to date, is needed. ELBNE is developing a scalable far detector design shown in Figure 5 that would scale-up LAr TPC technology by roughly a factor of 50 compared to the ICARUS T600 detector. To achieve this scale-up, a

number of novel design elements need to be employed. A membrane cryostat typical for the liquefied natural gas industry will be used instead of a conventional evacuated cryostat. The wire planes or anode plane assemblies (APAs) will be factory-built as planar modules that are then installed into the cryostat. The modular nature of the APAs allow the size of the detector to be scaled up to at least 40 kt fiducial mass. Both the analog and digital electronics will be mounted on the wire planes inside the cryostat in order to reduce the electronic noise, to avoid transporting analog signals large distances, and to reduce the number of cables that penetrate the cryostat. The scintillation photon detectors will employ light collection paddles to reduce the required photo-cathode area. Many of the aspects of the design will be tested in a small scale prototype at Fermilab but given the very large scale of the detector elements a full-scale test is highly desirable.

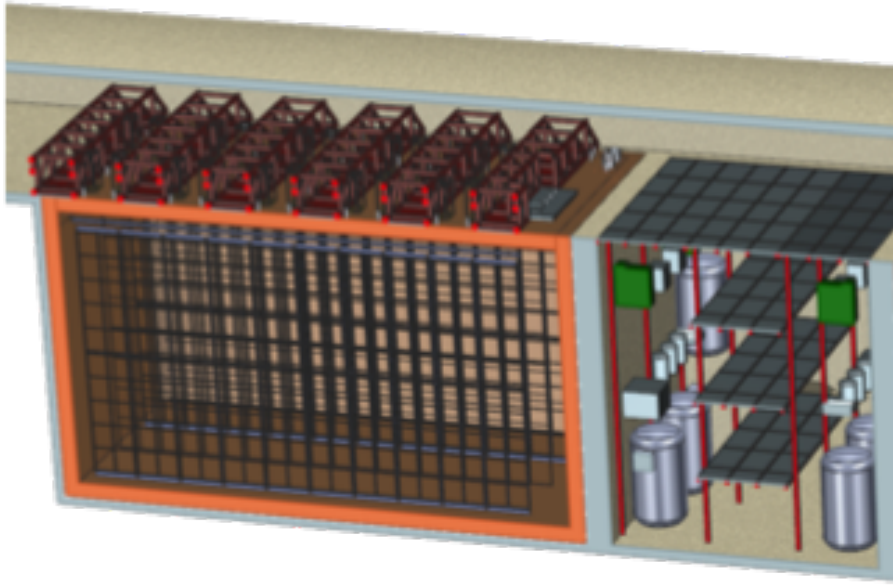


Figure 5: 3D model of one design of the ELBNF single-phase detector. Shown is 5kt fiducial volume detector which would need to be lengthened for the 10 kt design. The present ELBNF plan calls for the construction of 4 10 kt detectors of similar design.

The goals of the LBNE detector test can be broken into four categories: argon contamination mitigation verification, TPC mechanical verification, TPC electrical verification, and photon detection light yield verification. Research at Fermilab utilizing the Materials Test Stand has shown that electronegative contamination to the ultra-pure argon from all materials tested is negligible if the material is under the liquid argon. This implies that the dominant source of contamination originates from the gas ullage region and in the room temperature connections to the detector. Careful design of the ullage region to insure that all surfaces and feedthroughs are cold is expected to greatly reduce the sources of contamination over what exists in present detectors. Other concepts attempt to eliminate the gas ullage completely. The goals related to mechanical testing are to test the integrity of the detec-

tor. In the current design, each APA measures 2.3 m by 6.0 m and includes 2560 wires and associated readout channels. Given the complexity of these assemblies, a test where the detector can be thermally cycled and tested under operating conditions is highly advised prior to mass production. The mechanical support of the APAs can be tested to verify that the mechanical design is reliable and will accommodate any necessary motion between the large wire planes. The impact of vibration isolation between the cryostat roof and the detector can also be tested. Finally a potential improvement in the cryostat design is the possibility to move the pumps external to the main cryostat. This will reduce any mechanical coupling to the detector and also greatly improve both reliability and ease of repair. The electrical testing goals are to insure that the high voltage design is robust and that the required low electronic noise level can be achieved. As the detector scale increases so does the capacitance and the stored energy in the device. The design of the field cage and high voltage cathode planes needs to be such that HV discharge is unlikely and that if the event occurs no damage to the detector or cryostat results. The grounding and shielding of large detectors is also critical for low noise operation. By testing the full scale elements one insures that the grounding plan is fully developed and functional. Large scale tests of the resulting design will verify the electrical model of the detector.

3.2 CERN prototype detector

3.2.1 Overview of the CERN test Detector

The TPC will be assembled from elements that are of the same size as those planned for the single phase far detector. The overall size of the TPC will be derived by the size and number of anode planes (APA). It has been determined in order to perform the required physics, the TPC will consist of three APAs. The APAs will have an active area 2.29 m wide and 6.0 m high. These active area dimensions result in an APA that is 2.32 m wide and 6.29 m high. The combination of the three APAs will determine the overall length of the TPC. This is 7.2 m. There will be a cathode plane (CPA) on either side of the APAs. The size of the CPAs is determined by the active area of the three APAs. The active area of the three APAs is approximately 7.2 m wide by 6.2 m high. The drift distance between the CPAs and row of APAs will be 2.5 m. The overall width of the TPC will be determined by a combination of the drift distances along with the thickness of the APA, which is constructed of 3" x 4" stainless steel (SS) structural tubing. The overall width of the TPC is 5.2 m. Like the length of the TPC, the overall height will be determined by the height of the APA. The overall height of the TPC will be 6.3 m. The TPC dimensions will be 7.2 m long x 5.2 m wide x 6.3 m high. Along with the APAs and CPAs, the TPC will include a field cage that surrounds the entire assembly. It will be designed similarly to the field cage in phase 2 of the 35t experiment at FNAL. This is a series of protruded fiberglass I beams for the structural elements. These I-beams will be tiled

with large copper sided FR4 panels to create the field cage. Each panel will be connected with a series of resistors. The field cage will be connected to the CPAs through a capacitor assembly.

All of this will be supported by rows of I-beams supported from a mechanical structure above the cryostat. The hangers for these I-beams will pass through the insulated top cap. There will be a series of feed thru flanges in the top cap of the cryostat to bring in and take out services for the TPC. There will be a HV feed thru for each of the CPAs and one signal feed thru for each of the APAs

Cryostat size from TPC dimensions (from Jack Fowler)

The minimum internal size of the cryostat is determined from size of the TPC. At the bottom of the cryostat there needs to be a minimum of 0.3 m between the frame of the CPA and closest point on the SS membrane. This is to prevent high voltage discharge between the CPA and the electrically grounded membrane. It is foreseen that there would be some cryogenic piping and instrumentation under the TPC. There is a height allowance of 0.1 m for this. There will be access and egress space around the outside of the TPC and the membrane walls. On three sides, 1.0 m of space is reserved for this. The final side of the TPC will have piping and instrumentation for the cryogenic system. There will be 1.3 m of space reserved for this.

The support system for the TPC will be located at the top between the underside of the cryostat roof and the top of the TPC. The plan is to model this space similar to what is planned for the far site TPC. There will be 0.9 m of ullage space. In order to prevent high voltage discharge, the upper most part of the CPA needs to be submerged a minimum of 0.3 m below the liquid Argon surface. The top of the TPC will be separated from the membrane by a minimum of 1.2 m.

Adding all of these to the size of the TPC yields the minimum inner dimensions of the cryostat. A minimally sized cryostat would be 9.5 m long, 7.3 m wide and 8.4 m high. This assumes the TPC will be positioned inside the cryostat with the CPAs and end field cages parallel to the walls of the cryostat. Also there is no space allotted for a beam window to enter the cryostat. Clearance would need to be added if it violates any of the current boundaries listed above. These dimensions also preserve the ability to reverse the order of the APAs and CPAs inside the TPC. The current plan is to have the APAs located in the center of the cryostat with a CPA on each side. Reversing this to have the CPA in the center and APAs on each side may be required to achieve some of the proposed physics. The orientation of the TPC components will be finalized after various scenarios have been sufficiently simulated.

3.2.2 Parameters table

3.2.3 Requirements (data rate, dimensions, gap to wall, ?)

3.2.4 Installation

Installation Plans for the TPC into the Cryostat (from Jack Fowler)

The interior of the cryostat will be prepared prior to the installation of the TPC. A series of support rails will be suspended below the top surface of the cryostat membrane. These will be structurally supported by a truss structure above the cryostat. These supports will pass through the top of the cryostat. They need to be designed to minimize the heat gain into the cryogenic volume. For the CPAs, the rails need to be electrically isolated due to high voltage concerns. To preserve the ability to reverse the order of the TPC components, all of the support rails will be designed to the same set of requirements regarding loads and attachment points.

There will be a series of feed thru flanges located along each of the support rails. These will be cryogenic flanges where the services for the TPC components can pass through the top of the cryostat. It is foreseen that each CPA will require one feed thru for the high voltage probe to bring in the drift voltage. The drift voltage is 500 V/cm. For a drift distance of 2.5 m, the probe voltage will be 125 kV. There will be one service feed thru for each of the APAs. These feed thrus will include high speed data, bias voltages for the wire planes, control and power for the cold electronics.

The main TPC components will be installed through a large hatch in the top of the cryostat. This is similar to the installation method intended for the detector at the far site. This hatch will have an aperture approximately 2.0 m wide and 3.5 m long. Each APA and CPA panel will be carefully tested after transport into the clean area and before installation into one of the cryostats. Immediately after a panel is installed it will be rechecked. The serial installation of the APAs along the rails means that removing and replacing one of the early panels in the row after others are installed would be very costly in effort and time. Therefore, to minimize the risk of damage, as much work around already installed panels as possible will be completed before proceeding with further panels. The installation sequence is planned to proceed as follows:

1. Install the monorail or crane in the staging area outside the cryostat, near the equipment hatch.
2. Install the relay racks on the top of the cryostat and load with the DAQ and power supply crates.
3. Dress cables from the DAQ on the top of the cryostat to remote racks.
4. Construct the clean-room enclosure outside the cryostat hatch.
5. Install the raised-panel floor inside the cryostat.

6. Insert and assemble the stair tower and scaffolding in the cryostat.
 7. Install the staging platform at the hatch entrance into the cryostat.
 8. Install protection on (or remove) existing cryogenics instrumentation in the cryostat.
 9. Install the cryostat feedthroughs and dress cables inside the cryostat along the support beams.
10. Install TPC panels:
- (a) Install both CPA panels. These will be installed from the floor of the cryostat. Access to the top edge will be required by scaffolding.
 - (b) Install and connect HV probe for each of the CPAs.
 - (c) Perform electrical tests on the connectivity of the probe to the CPAs.
 - (d) Install first end wall of vertical field cage at the non-access end of the cryostat. These will be installed from the floor of the cryostat. Scaffolding will be needed to install the supporting structure and then attach the panels to the structure.
 - (e) Test the inner connections of the field cage panels.
 - (f) Install the first APA and connect to the far end field cage support.
 - (g) Connect power and signal cables. This will require scaffolding to access the top edge of the APA.
 - (h) Test each APA wire for expected electronics noise. Spot-check electronics noise while cryogenics equipment is operating.
 - (i) Install the upper field cage panels for the first APA between the APA and CPAs. This will require scaffolding to access the upper edge of the APA, CPA and field cage structure.
 - (j) Perform electrical tests on upper field cage panels.
 - (k) Repeat steps (f) through (j) for the next two APAs.
 - (l) Install the lower field cage panels between the APAs and CPAs. Start at the far end away from the access hatch and work towards the hatch.
 - (m) Perform electrical test on lower field cage panels and the entire loop around the TPC.
 - (n) Remove temporary floor sections as the TPC installation progresses.
 - (o) Install sections of argon-distribution piping as the TPC installation progresses.
 - (p) Install the final end wall of vertical field cage at the access end of the cryostat. These will be installed from the floor of the cryostat. Scaffolding will be needed to install the supporting structure and then attach the panels to the structure.

11. Remove movable scaffold and stair towers.
12. Temporarily seal the cryostat and test all channels for expected electronics noise.
13. Seal the access hatch.
14. Perform final test of all channels for expected electronics noise.

In general, APA panels will be installed in order starting with the panel furthest from the hatch side of the cryostat and progressing back towards the hatch. The upper field cage will be installed in stages as the installation of APAs and CPAs progresses. After the APAs are attached to the support rods the electrical connections will be made to electrical cables that were already dressed to the support beams and electrical testing will begin. Periodic electrical testing will continue to assure that nothing gets damaged during the additional work around the installed APAs.

The TPC installation will be performed in three stages, each in a separate location; the locations, or zones, are shown in Figure x-xx (this illustration was made for a 34-kton, in-line underground detector, but the work zones are also applicable for the 10-kton surface siting). First, in the clean room vestibule, a crew will move the APA and CPA panels from storage racks, rotate to the vertical position and move them into the cryostat. Secondly, in the panel-staging area immediately below the equipment hatch of the cryostat, a second crew will transfer the lower panels from the crane to the staging platform, connect the upper and lower panels together, route cables to the top of stacked panels and finally transfer the stacked panels on to the monorail trolley that moves within the cryostat. A third crew will reposition the movable scaffolding and use the scaffold to make the mechanical and electrical connections at the top for each APA and CPA as they are moved into position. The monorails inside and outside the cryostat will each have two motorized trolleys so that work can be conducted by all three crews in parallel. The steady-state rate for installation, given this work plan and a single-shift schedule, is estimated to be two stacked panels per day.

The requirements for alignment and survey of the TPC are under development. Since there will be plenty of cosmic rays in the surface detector and beam events, significant corrections can be made for any misalignment of the TPC. The current plan includes using a laser guide or optical transit and the adjustment features of the support rods for the TPC to align the top edges of the APAs in the TPC to be straight, level and parallel within a few mm. The alignment of the TPC in other dimensions will depend on the internal connecting features of the TPC. The timing of the survey will depend on understanding when during the installation process the hanging TPC elements are in a dimensionally stable state. The required accuracy of the survey is not expected to be finer than a few mm.

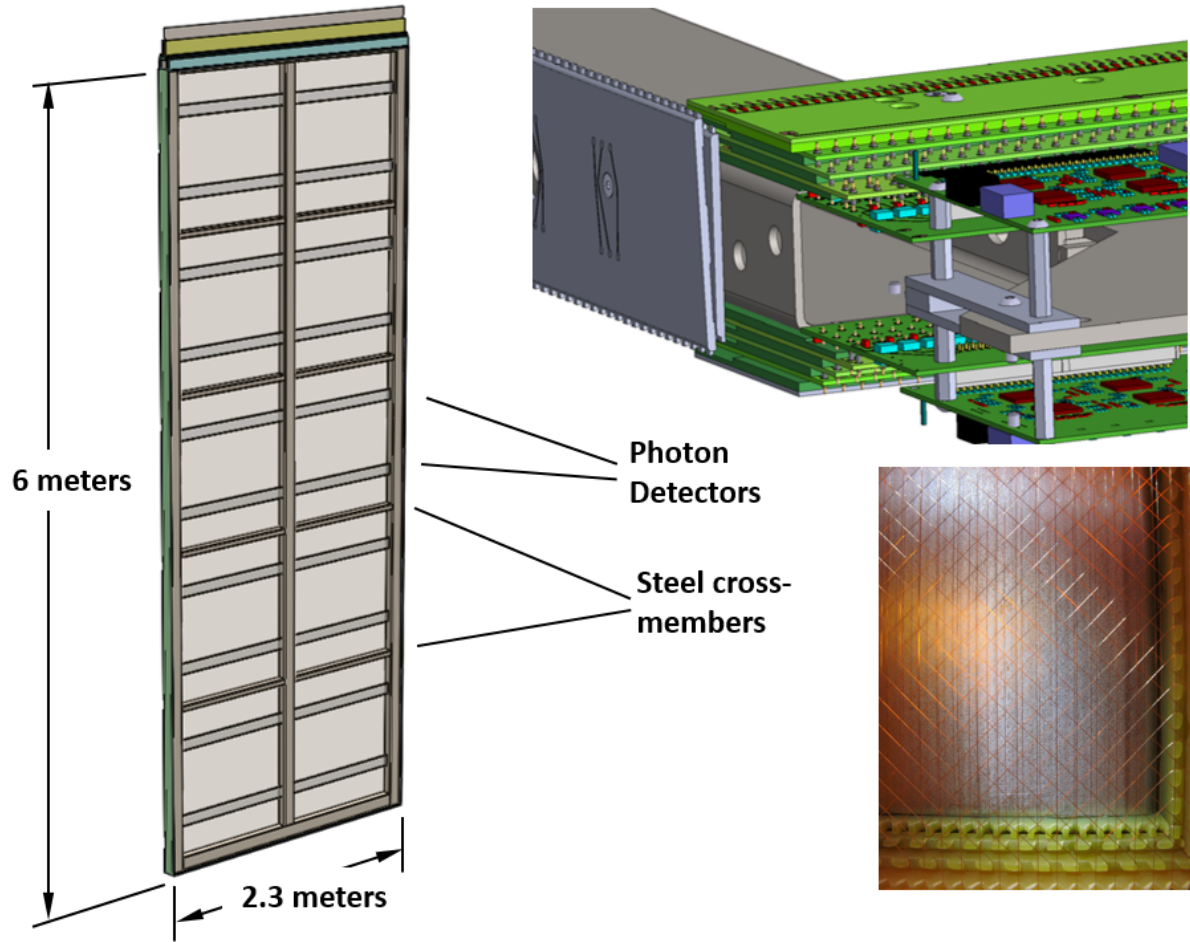


Figure 6: Clockwise from left: A full size APA, an APA corner showing the electronics boards, an APA lower corner photo showing wires and edge boards.

3.2.5 APA

The TPC consists of alternating anode plane assemblies (APAs) and cathode plane assemblies (CPAs), with field-cage panels enclosing the four open sides between the anode and cathode planes. A uniform electric field is created in the volume between the anode and cathode planes. A charged particle traversing this volume leaves a trail of ionization. The electrons drift toward the anode plane, which is constructed from multiple layers of sense wires, inducing electric current signals in the front-end electronic circuits connected to the wires.

The APAs are 2.3 m wide, 6 m long (plus an additional 0.3m of electronics), and 12 cm thick (Fig. 3.2.5). The 6 m length is a balance between maximizing the area per APA and making them a practical length for fabrication, transportation and maneuvering into final position in the TPC cryostat.

The 2.3 m width is chosen to fit in a standard HiCube shipping container for storage and transport. The underlying structure of each APA is a frame-

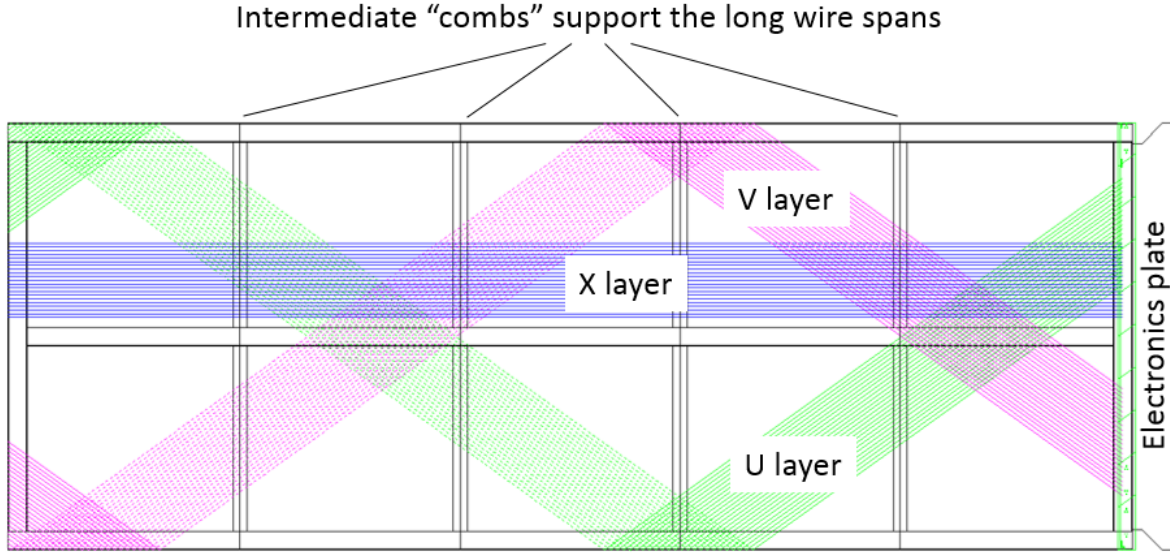


Figure 7: There are 3 instrumented layers of signal wires, one longitudinal and two angled, on each side of the APA which unambiguously locate an incident electron. The angled layers start at the electronics end and wind around to the other side on their way to the bottom. Partial layers are shown here; each layer fills the APA area completely. There is a fourth layer not shown (the G layer), above the instrumented layers that helps maintain the field.

work of rectangular, stainless steel tubing. The side and bottom edges of the frame are lined with multiple layers of fiberglass circuit boards, notched along the edges to support and locate the wires that cross the APA face. The front-end electronics boards are mounted at the top end of the frame and protected by a metal enclosure.

Four planes of wires cover each side of the APA frame (Fig. 3.2.5). The inner three planes of wires are instrumented and are oriented, going from the inside out: longitudinally, and at $\pm 35.7\text{deg}$ to the long axis, respectively. Each wire is connected to a front-end readout channel. These three planes of sense wires provide redundancy against the occasional dead channel and ensure reliable 2D position reconstruction regardless of track angles. The wires on the outermost plane are oriented longitudinally. They shield the inner sense wires and are not connected to the readout electronics. With a wire pitches of 4.67 mm (diagonal layers) and 4.79 (straight layers), the total number of readout channels in an APA is 2560.

The distance between wire planes is 4.8 mm (3/16 in) corresponding with standard printed circuit board thickness, and while maintaining optimal signal formation. The four wire planes will be electrically biased so that electrons from an ionizing-particle track completely drift past the first three planes and are collected by the fourth plane. Calculations show that the minimum bias voltages needed to achieve this goal are $V_G = -665\text{V}$, $V_U = -370\text{V}$, $V_V = 0\text{V}$ and $V_X = 820\text{V}$ respectively (where G, U, V, and X are the

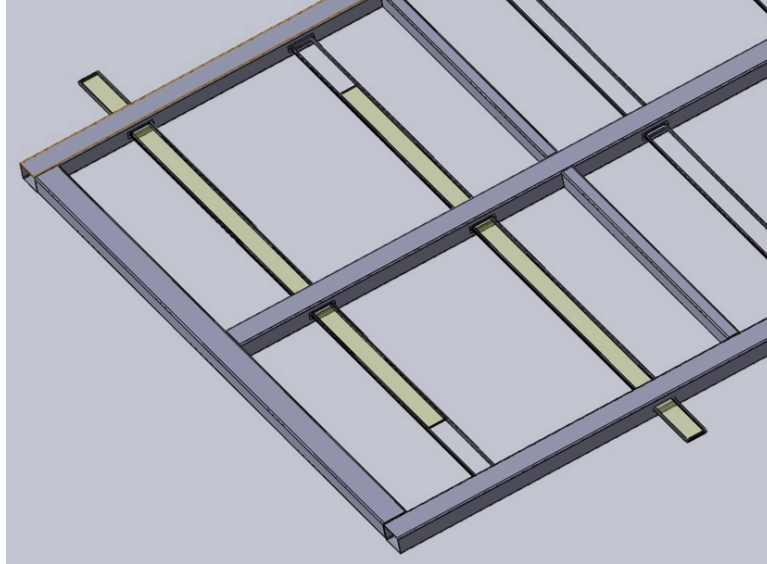


Figure 8: Photon detectors are mounted within the frame, between the wires on the two sets of four wire layers. The APA is built so that the photon detectors can be installed through slots in the side of the APA after the APA wires are installed. The wires that would cross these slots are routed around using copper traces on the edge boards.

wire-layer labels from outside in, towards the frame). It is convenient to set one of the wire planes to ground so that the wires can be DC coupled to the front-end readout electronics. In this instance, the V wire plane is set to ground potential to reduce the maximum bias voltages on the other wire planes, and enable the use of lower voltage rated AC coupling capacitors. A grounded mesh plane, located 4.8 mm behind the collection (X) plane, prevents the electric field around this set of wires from being distorted by the metal frame structure and the wires on the opposite side of the frame. It also shields the sensing wires from potential EM interferences from the photon detectors (Fig. 3.2.5) mounted within the frame. The mesh should have a wire pitch less than 2 mm to ensure a uniform electric field while maintaining a high optical transparency.

3.2.6 CPA and Field Cage

Each cathode plane (Fig. 9) is constructed from 6 identical CPA (cathode plane assembly) modules and two sets of end pieces. Each CPA is about half the size of an APA ($2.3\text{m} \times 3.1\text{m}$) for ease of assembly and transport. The CPA is made of a stainless-steel framework, with 4 pieces of thin FR4 sheets mounted in the openings. A receptacle for the HV feedthrough is attached to the upper corner of a cathode plane toward the roof entrance side to mate with the HV feedthrough in the cryostat ceiling.

The FR4 sheets on the CPAs are treated with layers of high resistive coating on both sides. The resistivity of the coating will be chosen such that the surface potential does not deviate significantly with the ionization

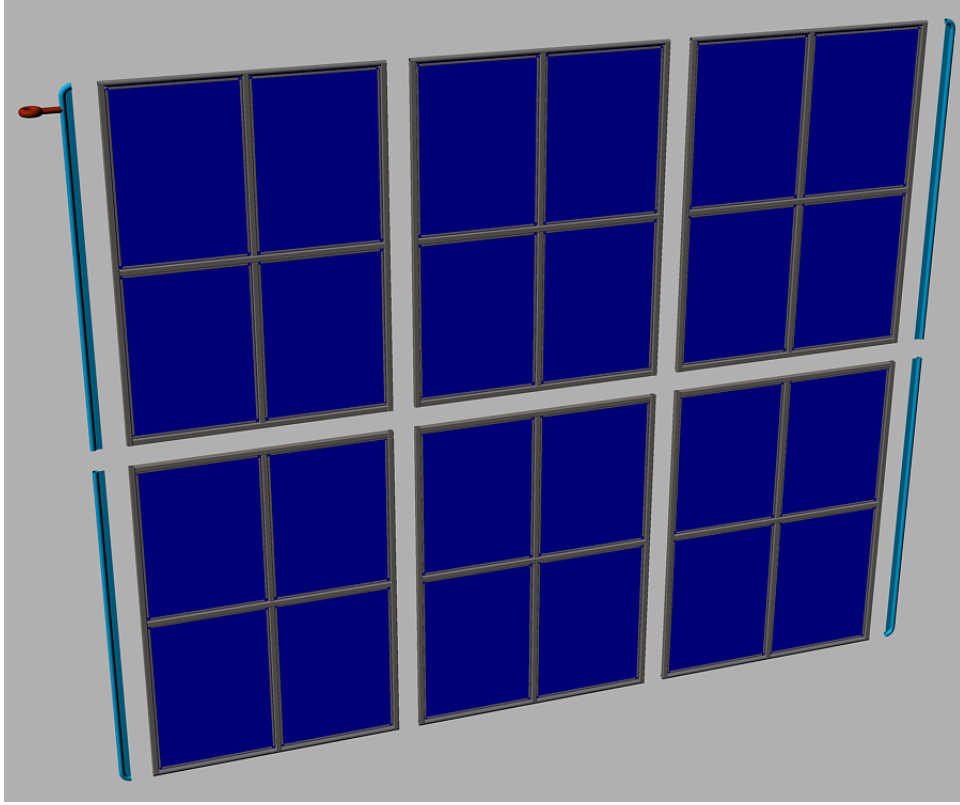


Figure 9: Exploded view of a cathode plane constructed from 6 CPA modules and 4 end pieces. The facing material on the CPA is highly resistive to minimize the peak energy transfer in case of a HV breakdown.

current from the cosmic rays, and forms a relatively long time constant to dissipate the stored energy on each sheet in case of a high voltage discharge. This long RC time constant will also reduce the peak current injected into the front-end electronics in a HV discharge.

Due to the relatively high cosmic ray flux in this surface detector, it is preferable to prevent the scintillation light emitted by a cosmic ray between the cathode and cryostat wall from entering the TPC to reduce false trigger. The opaque cathode surface will service this purpose. The high flux of cosmic rays combined with very low drift velocity of positive ions in the liquid argon will result in sizable space charge distortions in the TPC (docdb #6471). In addition, the positive ions could build up further if the ion motion is slowed or stalled by counter flow in the LAr. Preliminary CFD analysis (docdb #6140) have shown that solid cathodes in the cryostat result in LAr flow pattern that neither causes excess positive ion buildup, nor degrades the LAr purity.

To achieve a 500 V/cm drift field over a 2.5 m distance, the bias voltage on the cathode plane must reach -125 kV. Two high voltage power supplies ($150 - 200$ kV) and two HV feedthroughs will be needed for the two cathode planes. The HV feedthroughs are based on the Icarus design, but modified to further improve their stability at higher voltages (Fig. 10).

Each pair of facing cathode and anode rows forms an electron-drift region. A field cage completely surrounds the four open sides of this region to provide the necessary boundary conditions to ensure a uniform electric field within, unaffected by the presence of the cryostat walls.

The field cages are constructed using copper-clad FR4 sheets reinforced with fiber glass I-beams to form panels of $2.5\text{ m} \times 2.3\text{ m}$ in size for the top and bottom modules, and $2.5\text{ m} \times 2\text{ m}$ modules for the sides. Parallel copper strips are etched or machined on the FR4 sheets. Strips are biased at appropriate voltages through a resistive divider network. These strips will create a linear electric-potential gradient in the LAr, ensuring a uniform drift field in the TPC's active volume.

Since the field cage completely encloses the TPC drift region on four (of six) sides, with the remaining two sides blocked by the solid cathodes, the FR4 sheets must be frequently perforated to allow natural convection of the liquid argon. The “transparency” of the perforation will be determined by a detailed LAr computerized fluid dynamic (CFD) study.

Figure 11 shows a section of the field cage in the 35ton TPC as it was being assembled. The 35ton TPC test results will inform us whether we should improve upon the current design, or change the design concept all together for this and future detectors. The main concern with the current field cage design is that the electric field at the edges of the copper strips is still quite high due to the thinness of the copper. One possible remedy is to cover the entire surface of the field cage with a high resistive coating. The resistivity between strips due to this coating must be kept many orders of magnitudes higher than the divider resistance to avoid distortion to the drift field. Figure 12 shows a FEA of such a configuration.

In the event of HV discharge on the cathode or the field cage, the voltage differential between neighboring field cage strips near the discharge electrode will be very high for a brief moment. This over voltage condition could cause damage to the field cage electrode and the resistors installed between strips. To minimize such risk, varistors or gas discharge tubes (GDT) will be installed between the field cage strips in parallel with the resistors to prevent excess voltage transient between the electrodes.

In order to test the installation concept of the far detector, the top and bottom field cage modules will be attached to the mating CPAs through hinges. These combined assembly will be installed into the cryostat and the field cage module opens to bridge the CPA and the APA both mechanically and electrically.

Figure 10: Cross section of the HV feedthrough around the end of the grounded shield, and plot of the equi-potential contours between the HV central conductor and the ground shield. The flared end significantly reduces the electric field at the inside of the shield, improving HV stability.



Figure 11: A section of the field cage in the 35ton TPC

3.2.7 TPC Readout

The TPC front-end (FE) electronics operate at cryogenic temperatures. The system provides amplification, shaping, digitization, buffering and multiplexing of the signals. The FE electronics consist of three boards stacked on top of one another: the Analog Mother Board, the FPGA Mezzanine Board, and the SERDES Mezzanine Board. Figure 3.2.7 shows a schematic of the cold FE electronics.

The Analog Mother Board contains the front-end ASIC chips which perform the analog readout of the TPC wires. The FE ASIC chip is implemented as a mixed-signal ASIC providing amplification, shaping, digitization, buffering, a 16:2 multiplexing stage, a driver and voltage regulators. The analog-to-digital converter on the ASIC samples each TPC wire at 2 MHz. Eight such chips are mounted on a single readout board, instrumenting 128 adjacent wires in one plane.

The two (multiplexed) signals from each FE ASIC are fed into the FPGA Mezzanine Board. The cold FPGA aggregates the TPC data and also supplies the control and clock to the FE ASICs. The FPGA on the mezzanine board receives the data and packages the 128 channels together, one 2 MHz clock tick at a time. This is then sent to the SERDES board for serialization and sent to the cryostat flange board over high-speed (1 Gbps) serial links and finally to the DAQ system.

Besides the high-speed signal cable, which is a twin-axial cable bundle manufactured by GORE, there are cable bundles for low-voltage power, wire-bias voltages, and various slow controls and monitoring. Redundant cables will be provided for many of these functions. The cable bundles will be connected through a feedthrough on the roof of the cryostat.

| parameter | value |
|-------------------------------|------------|
| ADC Sampling Rate | 2 MHz |
| More stuff | |
| Cluster-on-Boards (COB) | 3 |
| Data-Processing-Modules (DPM) | 12 |
| ATCA Shelves | 1 (6-slot) |
| TPC Readout Compute Nodes | 3 |

The primary interface between the TPC front-end electronics (FE) and the DAQ subsystem consists of an ATCA-based system of RCEs (Reconfigurable Cluster Elements). The RCE system receives the serialized raw data for the FE, performs zero-suppression on it, and packetizes and transmits the resulting sparsified data to a back-end data farm for event building and further processing. Additionally, the RCE system transmits timing and control signals to the FE as well as forwarding configuration data to them at start-up.

The RCE system consists the following components: a commercial ATCA shelf (2-, 6-, or 14-slot), a Cluster-On-Board (COB) which is the "front board" in ATCA terms, and a Rear-Transition-Module (RTM) which is the "rear board". A schematic of the system is shown in Figure 3.2.7. The COB is a custom board, developed by SLAC, which holds the processing power of the system. The COB (see Figure ??) consists of 5 bays for holding daughter boards, an onboard 10-GbE switch, and both 10- and 1-Gb ethernet connections for communications with the back-end system. Four of the daughter-board bays are for Data Processing Modules (DPM), each of which can hold up to two RCEs. The RCE is the core procession unit of the system; it is made up of a modern SoC (currently, the Xilinx Zynq-7045) with multiple high-speed I/O ports (up to 10-Gbps each) and external DRAM and flash memory controllers. The other bay on the COB contains the Data Transmission Module (DTM) which is responsible for distributing timing and trigger information to and between the DPMs.

While the COB hardware is application agnostic, the RTM is application specific. The RTM provides the mechanical interface between the front-end (or, in our case, the flange electronics) and the back-end, as well as other external sources such as the timing or trigger systems. In this case we will use fiber optic connections between the flange and the TPC DAQ using 8 12-channel (full duplex) CXP connectors on the RTM.

With the assumption that each cold FE board multiplexes it's 128 wire channels to 4 outputs at 1-Gbps each, the non-zero suppressed data for 1 APA can be fed into a single COB (containing 8 RCEs). Each RCE would receive data from 2 FE boards, perform zero-suppression, and send the result to the back-end.

MG***data rates?

3.2.8 Photon Detection System

4 Photon Detector

This section to provide context and illustrate which aspects need testing at the cERN prototype

4.1 Introduction

The ELBNF far detector will utilize liquid argon scintillation light to determine the prompt event time of beam-driven and non-beam events. While the TPC will have far superior spatial resolution to a photon detection system, the drift time for TPC events is on the order of milliseconds. The beam clock will give much better timing resolution than this but a photon detection system can determine the start of an event occurring in the TPC volume (or entering the volume) to about 6 ns, which will be useful in determining the t_0 of cosmic ray events, events from radiological decays, and corrections to energy loss of the drifting electrons.

A charged particle passing through liquid argon will produce about 40,000 128 nm photons per MeV of deposited energy. At higher fields this will be reduced due to reduced recombination, but at 500 V/cm the yield is still about 20,000 photons per MeV. Roughly 1/3 of the photons are prompt 2-6 ns and 2/3 are generated with a delay of 1100-1600 ns. LAr is highly transparent to the 128 nm VUV photons with a Rayleigh scattering length and absorption length of 95 cm and \sim 200 cm respectively.

The relatively large light yield makes the scintillation process an excellent candidate for determination of t_0 for non-beam related events. Detection of the scintillation light may also be helpful in background rejection.

Several prototypes of photon detection systems have been developed by the LBNE, now ELBNF, photon detector group over the past few years. There are currently three prototypes under consideration for use in the ELBNF far detector, a baseline design along with two alternate designs. A decision on the final design will be made in September 2015. The CERN neutrino platform ELBNF test would provide the first full scale test of the ELBNF photon detector fully integrated into a full scale TPC anode plane assembly.

4.2 Baseline Design (TPB-Coated Acrylic Bars)

The reference design for the photon detection system is based on acrylic bars that are 200 cm long and 7.63 cm wide, which are coated with a layer of tetraphenyl-butadiene (TPB). The wavelength shifter converts VUV (128 nm) scintillation photons striking it to 430 nm photons inside the bar, with an efficiency of 50% of converting a VUV to an optical photon. A fraction of the wavelength-shifted optical photons are internally reflected to the bar's end where they are detected by SiPMs whose QE is well matched to the

430 nm wavelength-shifted photons. All PD prototypes are currently using SensL MicroFB-6K-35-SMT 6 mm × 6 mm devices.

A full 6 m long APA will be divided into 5 bays with 2 PD modules (paddles) instrumenting each bay (Fig. 1). The paddles will be inserted into the frames after the TPC wires have been wrapped around the frames allowing final assembly at the CERN test location. Two alternative designs are also under consideration.

4.3 Alternate 1: Coated Acrylic Plate with Fiber Readout

The first alternate design was motivated by a potential increase in the geometrical acceptance of the photon detectors. The number of required SiPMs and readout channels per unit detector area covered with photon detection panels would be significantly reduced to keep the overall cost for the photon detection system at or below the present design while increasing the geometrical acceptance at the same time.

The prototype consists of a TPB-coated acrylic panel embedded with an S-shaped wavelength shifting (WLS) fiber. The fiber is read out by two SiPMs, which are coupled to either end of the fiber and serves to transport the light over long distances with minimal attenuation. The double-ended fiber readout has the added benefit to provide some position dependence to the light generation along the panel by comparing relative signal sizes and arrival times in the two SiPMs. Figure 2 shows a schematic of the layout and a picture of a prototype PD paddle.

4.4 Alternate 2: Fiber Bundle with TPB-coated radiator

Motivated by increasing the attenuation length of the PD paddles and allowing collection of 400 nm photons coming from anywhere in the active volume of the TPC, the fiber-bundle design utilizes a TPB-coated radiator situated in front of a bundle of wavelength-shifting fibers (Fig. 3).

The fiber-bundle design is based on a thin TPB coated acrylic radiator located in front of a close packed array of WLS fibers. This concept is designed so that roughly 1/3 of the photons converted in the radiator are incident on the bundle of fibers, which are directed onto SiPMs at one end. The wavelength shifting fibers are Y11 UV/blue

from Kuraray and have mean absorption and emission wavelengths of about 440 nm and 480 nm respectively. The attenuation length of the Y11 fibers is given to be greater than 3.5 m at the mean emission wavelength, which will allow production of full-scale (2 m length) photon detector paddles.

4.5 Technology Selection

The PD system tested at the CERN neutrino platform will be based on technology selected later this year. The technology selection process will

be based on a series of tests planned for the next 6 months utilizing large research cryostats at Fermilab and Colorado State University. The primary metric used for comparison between the three technologies will be photon yield per unit cost. In addition to this metric PD threshold and reliability will also serve as inputs to the final decision. A technical panel will be assembled to make an unbiased decision.

Once the technology has been chosen the PD group will focus on optimizing the selected design with the goal of procurement and assembly taking place in late FY 2016 and early FY 2016. The photon detector paddles will then be tested and shipped to CERN in early FY 2017 for installation into the APAs in late FY 2017 in preparation for installation into the test cryostat and operation in 2018.

4.5.1 DAQ, Slow control and monitoring

The DAQ will merge data to form events from the LArTPC, photon detector and beam detector readouts using the artDAQ data acquisition toolkit using a farm of commercial computers connected with an Ethernet switch. ArtDAQ is in use on several experiments at Fermilab. We are using it on the 35t prototype, so we will have considerable experience by the time of the CERN test.

The data collection for the CERN test will operate in a mode similar to that foreseen for the underground detectors. In order to collect data from non-beam interactions such as proton decay candidates or atmospheric neutrinos, data will be continuously read in to the artDAQ data receiver nodes and processed through the artDAQ system in quanta corresponding to time intervals fixed from the time of the beginning of the run. These are then transferred through the switch to a set of event building nodes which work in parallel, each node receiving all the data from all the detectors for the time intervals it is responsible for processing. There will be 32 parallel incoming data streams from the LArTPCs and 16 streams from the photon detectors. There will be an additional stream from the trigger board (the same board as built by Penn for the 35t test will be used) which will receive input of the spill gate, warning of extraction, and pattern-unit bits from trigger counters and other beamline instrumentation such as Cerenkov counters [Which section are these described in?, should we refer to them from here?].

Synchronisation across all the input sources is essential in order that artDAQ can bring together the data from the input streams correctly for processing by the event building nodes. The data receiver nodes will provide overlap by repeating the data at the boundaries of the time intervals so that a particle whose data spans two time intervals can be collected. The time synchronisation is provided to the RTM back-module on the LArTPC readout crates, to the SSP photon detector readout and to the trigger board from a GPS based time synchronisation distribution system originally designed for the NOvA experiment. This system includes functionality to calibrate and correct for the cable delays, and to send synchronisation control signals

to the readout at predetermined times.

The event building nodes will select time regions of interest within the time intervals they are processing and form these into events to be written to disk. The algorithms to select the events may be as simple as looking for a trigger bit in the trigger board data stream, or may involve looking for self-triggered events in the LArTPC data. An aggregation task, which is part of artDAQ will handle the parallelized event building processes by merging the output events into a single stream and writing them to disk. To avoid oversized output data files, when a predetermined file size is reached, the aggregator will switch to writing to a new file. The collaboration requests to CERN, data links of sufficient bandwidth to transfer these files from the CENF to the CERN data center, and from there to locations worldwide for analysis.

Improved versions of the software systems which are being prototyped at the 35t test will available for the CERN test including (a) Run control which controls and monitors the DAQ processes and allows run starts and stops to be performed by the operator (b) online monitoring (c) slow control of voltages and temperatures being used by the electronics (this may not be comprehensive by the time of the CERN prototype, but we plan on prototyping the readout of some of the quantities). The trigger board includes facilities for generating calibration pulses and for identifying the event times of the calibration events.

5 Cryostat and cryogenics system [~5 pages; **David/Barry/Jack**

Describe requirements to meet detector goals

5.1 LBNF detector

This section to provide context and illustrate which aspects need testing at the CERN prototype

(Probably can take text from CDR once it's more developed)

5.2 CERN prototype detector

5.2.1 Cryostat from David Montanari

The Single Phase TPC test at CERN will use a membrane tank technology to contain the base design of 725 tons of LAr equivalent to about $520m^3$. The design is based on a scaled up version of the LBNE 35 Ton Prototype and the Fermilab Short Baseline Near Detector. We propose that the cryostat be housed in the extension of the EHN1 Bat 887 at CERN, where the cryogenic system components will also be located. The cryostat will use a steel outer supporting structure with a metal liner inside to isolate the insulation volume, similar to the one of the dual phase detector prototype WA105 $1 \times 1 \times 3$ and to the Fermilab Short Baseline Near Detector. The support structure

will rest on I-beams to allow for air circulation underneath to maintain the temperature within the allowable limits. The scope of the EHN1 cryostat subsystem includes the design, procurement, fabrication, testing, delivery and oversight of a cryostat to contain the liquid argon and the TPC. This section describes a reference design, whose scope encompasses the following components:

- steel outer supporting structure,
- main body of the membrane cryostat (sides and floor),
- top cap of the membrane cryostat.

A membrane cryostat design commonly used for liquefied natural gas (LNG) storage and transportation will be used. In this vessel a stainless steel membrane contains the liquid cryogen. The pressure loading of the liquid cryogen is transmitted through rigid foam insulation to the surrounding outer support structure, which provides external support. The membrane is corrugated to provide strain relief resulting from temperature related expansion and contraction. The vessel is completed with a top cap that uses the same technology.

Two membrane cryostat vendors are known: GTT (Gaztransport & Technigaz) from France and IHI (Ishikawajima-Harima Heavy Industries) from Japan. Each one is technically capable of delivering a membrane cryostat that meets the design requirements for this detector. To provide clarity, only one vendor is represented in this document, GTT; this is for informational purposes only. Figure 1 shows a 3D model of the GTT membrane and insulation design.

The conceptual reference design for the Single Phase Test at CERN cryostat is a rectangular vessel measuring 9.5 m in length (parallel to the beam direction), 7.3 m in width, and 8.40 m in height; containing a total mass of 725 tons of liquid argon. Figure 18 shows side and end views of the cryostat respectively. Figure 3 shows a 3D view. To minimize the contamination from warm surfaces, during operation the temperature of all surfaces in the ullage shall be lower than 100 K. The top plate will contain two hatches to install the TPCs and enter the tank, a manhole and several penetrations for the cryogenic system and the detector.

Design Parameters (from David Montanari)

This design is meant to test technical solutions that may be of interest for future needs of the Long Baseline Neutrino program. The use of a cold ullage (<100 K) to lower the impurities in the gas region, and of a LAr pump outside the cryostat to minimize the effect of noise, vibration and microphonics to the TPC inside the LAr are Value Engineering studies for the Long Baseline program.

The design parameters for the TPC Test at CERN cryostat are listed in Table 3.

Insulation system and secondary membrane (from David Montanari)

Table 3: Design requirements for the cryogenic system (has right values)

| Design Parameter | Value |
|--|--|
| Type of structure | Membrane cryostat |
| Membrane material | SS 304/304L, 316/316L or equivalent. Other materials upon approval. |
| Outside reinforcement (support structure) | Steel enclosure with metal liner to isolate the outside from the insulation space, standing on legs to allow for air circulation underneath. |
| Total cryostat volume | 583 m3 |
| Total LAr volume | 520 m3 |
| LAr total mass | 725,000 kg |
| Minimum inner dimensions (flat plate to flat plate). | 7.3 m (W) x 9.5 m (L) x 8.4 m (H) |
| Depth of LAr | 7.5 m (0.9 m ullage, same as LBNF) |
| Primary membrane | 1.2 mm thick SS 304L corrugated stainless steel |
| Secondary barrier system | 0.07 mm thick aluminum between fiberglass cloth. Overall thickness 1 mm located between insulation layers. |
| Insulation | Polyurethane foam (0.8 m thick from preliminary calculations) |
| Maximum static heat leak | 15 W/m2 |
| LAr temperature | 88 +/- 1K |
| Operating gas pressure | Positive pressure. Nominally 70 mbarg (1 psig) |
| Vaccum | No vacuum |
| Design pressure | 350 mbarg (5 psig) + LAr head (1,025 mbarg) |
| Design temperature | 77 K (liquid nitrogen temperature for flexibility) |
| Temperature of all surfaces in the ullage during operation | |
| Leak tightness | <100 K |
| Maximum noise/vibration/microphonics inside the cryostat | LAr pump outside the cryostat |
| Beam window | In the center of the active volume. Precise location TBD. |
| Accessibility after operations | Capability to empty the cryostat in 30 days and access it in 60 days after the end of operations. |
| Lifetime / Thermal cycles | Consistent with liquid argon program. TBD. |

The membrane cryostat requires insulation applied to all internal surfaces of the outer support structure and roof in order to control the heat ingress and hence required refrigeration heat load. The maximum required static heat leak is $15W/m^2$ for the floor and the sides and $20W/m^2$ for the roof. Preliminary calculations show that it can be obtained using 0.8 m thick insulation panels. Given an average thermal conductivity coefficient for the insulation material of $0.0283\text{ W}/(\text{m}\cdot\text{K})$, the heat input from the surrounding steel is expected to be about 3.7 kW total. It assumes that the hatches are foam insulated as well. This is shown in Table 4.

The insulation material is a solid reinforced polyurethane foam manufactured as composite panels. The panels get laid out in a grid with 3 cm gaps between them (that will be filled with fiberglass) and fixed onto anchor bolts anchored to the support structure. The composite panels contain the two layers of insulation with the secondary barrier in between. After positioning adjacent composite panels and filling the 3 cm gap, the secondary membrane is spliced together by epoxying an additional overlapping layer of secondary membrane over the joint. All seams are covered so that the secondary membrane is a continuous liner.

The secondary membrane is comprised of a thin aluminum sheet and fiber-glass cloth. The fiberglass- aluminum-fiberglass composite is very durable and flexible with an overall thickness of about 1 mm. The secondary membrane is placed within the insulation space. It surrounds the bottom and sides. In the unlikely event of an internal leak from the primary membrane of the cryostat into the insulation space, it will prevent the liquid cryogen from migrating all the way through to the steel support structure where it would degrade the insulation thermal performance and could possibly cause excessive thermal stress in the support structure. The liquid cryogen, in case of leakage through the inner (primary) membrane will escape to the insulation volume, which is purged with GAr at the rate of one volume exchange per day.

Table 4: Heat load calculation for the membrane cryostat (insulation thickness = 0.8 m). (note to self: has right values)

| Element | Area (m^2) | K (W/mK) | $\Delta T (K)$ | Heat Input (W) |
|------------|----------------|--------------|----------------|----------------|
| Base | 83 | 0.0283 | 205 | 605 |
| End walls | 190 | 0.0283 | 205 | 1,374 |
| Side walls | 149 | 0.0283 | 205 | 1,081 |
| Roof | 83 | 0.0283 | 205 | 605 |
| Total | | | | 3,665 |

Cryostat Configuration (from David Montanari)

This section describes the configuration of the cryostat only. The TPC is described in Section xxx. With the intent to minimize the contamination

in the gas region, the ullage will be kept cold (<100 K). A possible way to achieve this requirement is to spray a mist of clean liquid and gaseous argon to the metal surfaces in the ullage and keep them cold, similar to the strategy that was developed for the cool down of the LBNE 35 Ton prototype.

Outer Support Structure (from David Montanari)

The reference design is a steel support structure with a metal liner on the inside to isolate the insulation region and keep the moisture out. This choice allows natural and forced ventilation to maintain the temperature of the steel within acceptable limits, without the need of heating elements and temperature sensors. It reduces the time needed for the construction: the structure will be prefabricated in pieces of dimensions appropriate for transportation, shipped to the destination and only assembled in place. Fabrication will take place at the vendor's facility for the most part. This shortens the construction of the outer structure on the detector site, leaving more time for completion of the building infrastructure. If properly designed, a steel structure may allow the cryostat to be moved, should that be desired later in the future.

Main body of the membrane cryostat (from David Montanari)

The sides and bottom of the vessel constitute the main body of the membrane cryostat. They consist of several layers. From the inside to the outside the layers are stainless steel primary membrane, insulation, thin aluminum secondary membrane, more insulation, and steel outer support structure with metal panels acting as vapor barrier. The secondary membrane contains the LAr in case of any primary membrane leaks and the vapor barrier prevents water ingress into the insulation. The main body does not have side openings for construction. The access is only from the top. There is a side penetration for the liquid argon pump for the purification of the cryogen.

Top cap (from David Montanari)

Several steel reinforced plates welded together constitute the top cap. The stainless steel primary membrane, intermediate insulation layers and vapor barrier continue across the top of the detector, providing a leak tight seal. The secondary barrier is not used nor required at the top. The cryostat roof is a removable steel truss structure that bridges the detector. Stiffened steel plates are welded to the underside of the truss to form a flat vapor barrier surface onto which the roof insulation attaches directly. The penetrations will be clustered in the back region, as far away from the beam as possible. The top cap will have a large opening for TPC installation, a secondary smaller opening for personnel access and a manhole.

The truss structure rests on the top of the supporting structure where a positive structural connection between the two is made to resist the upward force caused by the slightly pressurized argon in the ullage space. The hydrostatic load of the LAr in the cryostat is carried by the floor and the sidewalls. Everything else within the cryostat (TPC planes, electronics, sensors, cryogenic and gas plumbing connections) is supported by the steel plates under the truss structure. All piping and electrical penetration into the interior of the cryostat are made through this top plate, primarily in the region of the

penetrations to minimize the potential for leaks. Studs are welded to the underside of the top plate to bolt the insulation panels. Insulation plugs are inserted into the bolt-access holes after panels are mounted. The primary membrane panels are first tack-welded then fully welded to complete the inner cryostat volume.

Table 5 presents the list of the design parameters for the top of the cryostat.

Cryostat grounding and isolation requirements (from David Montanari)

The cryostat has to be grounded and electrically isolated from the building. This section presents the list of the current grounding and isolation requirements for the cryostat. Figure 19 shows the layout of the top plate grounding.

Isolation

1. The cryostat membrane and any supporting structure, whether it is a steel structure or a concrete and rebar pour, shall be isolated from any building metal or building rebar with a DC impedance greater than $300\text{ k}\Omega$.
2. All conductive piping penetrations through the cryostat shall have dielectric breaks prior to entering the cryostat and the top plate.

Grounding

1. The cryostat, or “detector” ground, shall be separated from the “building” ground.
2. A safety ground network consisting of saturated inductors shall be used between detector ground and building ground.
3. Parameters TBD.

Top plate grounding

1. If the cryostat is contained within a concrete pour, the top plate shall be electrically connected to any rebar used in that pour, and the rebar shall be conductively tied at regular intervals. Parameters TBD.
2. The top grounding plate shall be electrically connected to the cryostat membrane by means of copper braid connections.
 - (a) Each connection shall be at least 1.6 mm thick and 63.5 mm wide.
 - (b) The length of each connection is required to be as short as possible.
 - (c) The distance between one connection and the next one shall be no more than 1.25 m.
 - (d) The layout can follow the profile of several pieces of insulation, but it shall be continuous.
 - (e) The DC impedance of the membrane to the top plate shall be less than 1 ohm.

Table 5: Design parameters for the cryostat top (has right values)

| Design Parameter | Value |
|---|---|
| Configuration | Removable metal plate reinforced with trusses anchored to the membrane cryostat support structure. Contains multiple penetrations of various sizes and a manhole. Number, location and size of the penetrations TBD. Provisions shall be made to allow for removal and re-welding six (6) times. |
| Plate/Trusses non-wet material | Steel if room temperature. SS 304/304 or equivalent if at cryogenic temperature |
| Wet material | SS 304/304L, 316/316L or equivalent. Other materials upon approval. |
| Fluid | Liquid argon (LAr) |
| Design pressure | 350 mbarg (5 psig) |
| Design temperature | 77 K (liquid nitrogen temperature for flexibility) |
| Inner dimensions | To match the cryostat |
| Maximum allowable roof deflection | 0.028 m (span/360 from LBNF) |
| Maximum static heat leak | <20 W/m ² |
| Temperatures of all surfaces in the ullage during operation | <100 K |
| Additional design loads | <ul style="list-style-type: none"> - Top self-weight - TPC (3,000 kg on each anchor) - TPC anchors (TBD) - Live load (488 kg/m²) - Electronics racks (400 kg in the vicinity of the feed through) - Services (150 kg on every feed through) |
| TPC anchors | Capacity: 3,000 kg each anchor. Number and location TBD. Minimum 6. |
| Hatch opening for TPC installation | 3,550 m x 2,000 m (location TBD) |
| Grounding plate | 1.6 mm thick copper sheet brazed to the bottom of the top plate |
| Lifting fixtures | Appropriate for positioning the top at the different parts that constitute it. |
| Cold penetrations | Minimum 4 (??). Location and design TBD. |
| Lifetime / Thermal cycles | Consistent with the liquid argon program TBD. |

Leak prevention (from David Montanari)

The primary membrane will be subjected to several leak tests and weld remediation, as necessary. All (100%) of the welds will be tested by an Ammonia colorimetric leak test (ASTM E1066-95) in which welds are painted with a reactive yellow paint before injecting a Nitrogen-Ammonia mixture into the insulation space of the tank. Wherever the paint turns purple or blue, a leak is present. The developer is removed, the weld fixed and the test is performed another time. Any and all leaks will be repaired. The test lasts a minimum of 20 hours and is sensitive enough to detect defects down to 0.003 mm in size and to a $10^{-7} \text{ std } - \text{cm}^3/\text{s}$ leak rate (equivalent leak rate at standard pressure and temperature, 1 bar and 273 K). To prevent infiltration of water vapor or oxygen through microscopic membrane leaks (below detection level) the insulation spaces will be continuously purged with gaseous argon to provide one volume exchange per day. The insulation space will be maintained at 30 mbar, slightly above atmospheric pressure. This space will be monitored for changes that might indicate a leak from the primary membrane. Pressure control devices and safety relief valves will be installed on the insulation space to ensure that the pressure does not exceed the operating pressure inside the tank. The purge gas will be recirculated by a blower, purified, and reused as purge gas. The purge system is not safety-critical; an outage of the purge blower would have negligible impact on LAr purity.

Cryostat size from TPC dimensions (from Jack Fowler)

The minimum internal size of the cryostat is determined from size of the TPC. At the bottom of the cryostat there needs to be a minimum of 0.3 m between the frame of the CPA and closest point on the SS membrane. This is to prevent high voltage discharge between the CPA and the electrically grounded membrane. It is foreseen that there would be some cryogenic piping and instrumentation under the TPC. There is a height allowance of 0.1 m for this. There will be access and egress space around the outside of the TPC and the membrane walls. On three sides, 1.0 m of space is reserved for this. The final side of the TPC will have piping and instrumentation for the cryogenic system. There will be 1.3 m of space reserved for this.

The support system for the TPC will be located at the top between the underside of the cryostat roof and the top of the TPC. The plan is to model this space similar to what is planned for the far site TPC. There will be 0.9 m of ullage space. In order to prevent high voltage discharge, the upper most part of the CPA needs to be submerged a minimum of 0.3 m below the liquid Argon surface. The top of the TPC will be separated from the membrane by a minimum of 1.2 m.

Adding all of these to the size of the TPC yields the minimum inner dimensions of the cryostat. A minimally sized cryostat would be 9.5 m long, 7.3 m wide and 8.4 m high. This assumes the TPC will be positioned inside the cryostat with the CPAs and end field cages parallel to the walls of the cryostat. Also there is no space allotted for a beam window to enter the cryostat. Clearance would need to be added if it violates any of the

current boundaries listed above. These dimensions also preserve the ability to reverse the order of the APAs and CPAs inside the TPC. The current plan is to have the APAs located in the center of the cryostat with a CPA on each side. Reversing this to have the CPA in the center and APAs on each side may be required to achieve some of the proposed physics. The orientation of the TPC components will be finalized after various scenarios have been sufficiently simulated.

5.3 Cryogenic System (from David Montanari)

The cryogenic system is being developed as part of the international engineering team set up between Fermilab and CERN to design, fabricate and install cryogenic systems of similar requirements and increased size for Short and Long Baseline at Fermilab, and WA105s at CERN. The goal is to develop a single model and adapt if for all future generation detectors, with the necessary scaling up in size and adjustments for eventual different needs of the different detectors. Table 6 presents the list of requirements for the cryogenic system for the Single Phase TPC test at CERN detector.

Figure 20 outlines the basic scheme of the LN2 supply system, which was proposed by CERN for the Short Baseline Program and agreed as an appropriate solution for this detector as well. The experiment will rely on LN2 tankers for regular deliveries to a local dewar storage, which will be sized to provide several days of cooling capacity in the event of a delivery interruption. From the dewar storage the LN2 is then transferred to a distribution facility located in the experimental hall. It includes a small buffer volume and an LN2 pumping station that transfers the LN2 to the argon condenser and other services as needed. The low estimated heat leak of the vessel (3.5 kW) and the location inside an above ground building allow for use of an open loop system typical of other installations operated at Fermilab (LAPD, LBNE 35 ton prototype, MicroBooNE) and at CERN (???). Main goal of the LN2 system is to provide cooling power for the argon condenser, the initial cool down of the vessel and the detector, and all other services as needed.

Figure 21 shows a schematic diagram of the proposed liquid argon system. It is based on the design of the LBNE 35 ton prototype, the MicroBooNE detector systems and the current plans for the Long Baseline Far Detector.

Main goal of the LAr system is to purge the tank prior to the start of the operations (with GAr in open and closed loop), cool down the tank and fill it with LAr. Then continuously purify the LAr and the boil off GAr to maintain the required purity (electron lifetime measured by the detector).

The LAr receiving facility includes a storage dewar and an ambient vaporizer do deliver LAr and GAr to the cryostat. The LAr goes through the liquid argon handling and purification system, whereas the Gar through the gaseous argon purification before entering the vessel. The LAr purification system is currently equipped with a filter containing mol sieve and copper beds, and a regeneration loop to regenerate the filter itself. The filter medium may change following the ongoing developments on filtration

schemes, but the concept remains the same.

During operation, an external LAr pump circulates the bulk of the cryogen through the LAr purification system. The boil off gas is first re-condensed and then is sent to the LAr purification system before re-entering the vessel.

Table 6: Design requirements for the cryogenic system

| Parameter | Value |
|---|--|
| Location | Preferably not in front of the cryostat (on the beam) |
| Cooling Power | TBD based on the heat leak of the cryostat (estimated 3.5 kW), the cryo-piping and all other contributions (cryogenic pumps, etc.) |
| Liquid argon purity in cryostat | 10 ms electron lifetime (30 ppt O ₂ equivalent) |
| Gaseous argon piston purge rate of rise | 1.2 m/hr |
| Membrane cool-down rate | From manufacturer |
| TPCs cool-down rate | <40 K/hr, <10 K/m (vertically) |
| Mechanical load on TPC | The LAr or the gas pressure shall not apply a mechanical load to the TPC greater than 200 Pascal. |
| Nominal LAr purification flow rate (filling/ops) | 5.5 day/volume change |
| Temperature of all surfaces in the ullage during operations | <100 K |
| Gaseous argon purge within insulation | 1 volume change /day of the open space between insulation panels. |
| Lifetime of the cryogenic system | Consistent with the LAr program. TBD. |

6 Charged Particle Test Beam Requirements [~ 10 pages; Cheng-Ju]

6.1 Particle Beam Requirements

The requested beam parameters are driven by the requirement that the results from the CERN test beam should be directly applicable to the future large underground single-phase LAr detector with minimal extrapolation. The CERN test beam data will be used to evaluate the detector performance, to understand the various physics systematic effects, and to provide “neutrino-like” data for event reconstruction studies. The chosen beam parameters span a broad range of particle spectrum that are expected in the future neutrino experiment. The particle beam composition should consist of electrons, muons, and hadron beams that are charge-selected. The particle momentum of interest ranges from 0.2 GeV/c to 10 GeV/c. The maximum electron drift time in the TPC is about 3 ms. To minimize pile-up in the TPC, the desired beam rate should be around 200 Hz with the maximum rate below 300 Hz. The single-phase TPC consists of two drift volumes. It is desirable to aim the particle beam so that hadronic showers are mostly contained in the same drift volume. However, we also plan to take some data with hadronic shower crossing the midplane of the TPC from one drift volume to another. The two beam entry angles and positions with respect to the LAr cryostat are illustrated in Figure [XYZ.] The summary of the beam requirements are shown in Table 7.

Table 7: Particle beam requirements.

| Parameter | Requirements | Notes |
|------------------------|------------------------------------|--|
| Particle Types | e^\pm, μ^\pm, π^\pm | |
| Momentum Range | 0.2 - 10 GeV/c | |
| Momentum Spread | $\Delta p/p < 5\%$ | |
| Transverse Beam Size | RMS(x,y) < 2.5 cm | At the entrance face of the LAr cryostat |
| Beam Divergence | | |
| Beam Angle | $\approx 20^\circ$ | |
| Beam Dip Angle | -6° (nominal); $\pm 5^\circ$ range | |
| Beam Entrance Position | | |
| Rates | 200 Hz (average); 300 Hz (maximum) | |

6.2 EHN1 H4ext Beamline

The H4ext is an extension of the existing H4 beamline in Experimental Hall North 1 (EHN1). To produce particles in the momentum range of interest, 60 - 80 GeV/c pion beam from the T2 target is used to generate tertiary beams. The tertiary particles are momentum and charge-selected and transported

down H4ext beamline to the experimental area. A preliminary layout of the H4ext beamline is shown in Figure 22.

6.2.1 Beam Optics

[Waiting for inputs from Ilias]

6.2.2 Expected Rates and Purity

[Waiting for inputs from Ilias]

6.3 Beam Instrumentation

6.3.1 Beam Position Detector

6.3.2 Time-of-Flight Detector

6.3.3 Threshold Cherenkov Counter

6.4 Muon Beam Halo Counters

The halo counter is a set of plastic scintillator paddles surrounding the beamline. The main purpose is to tag particles (primarily muons from the upstream production target) that are outside of the beam axis, but may potentially enter the TPC volume. The counter information is used to either veto or simply flag these class of events.

6.5 Beam Window on LAr Cryostat

This section could be absorbed into the cryostat chapter.

7 Computing requirements, data handling and software [~3 pages; **Maxim Potekhin/Craig Tull**]

7.1 Overview

The proposed “Full Scale” test of a single-phase Liquid Argon TPC at CERN, performed in the context of the WA105 project and its evolution, will build upon the technology and expertise developed in the process of design and operation of its smaller predecessor, the 35t detector at FNAL. This includes elements of front-end electronics, data acquisition, run controls and related systems. We also expect that for the most part, Monte Carlo studies necessary to support this program will be conducted utilizing software evolved from tools currently used (2015).

In the test-beam setup, the detector performance will be characterized for different types of particles, e.g. p , π^\pm , μ^\pm etc. Current plans call for measurements in pre-defined bins of the incident particle momentum, which

will have widths ranging from tens to hundreds of MeV (see 7.2.4). The volume of data to be recorded shall be determined by the number of events that need to be collected in each measurements that provides adequately low statistical uncertainty of the parameters measured.

In our view, it is optimal to first stage the “precious” data collected from the prototype on disk at CERN and then sink it to tape (also at CERN), while simultaneously performing replication to data centers in the US. For the latter, FNAL is the prime candidate, with additional data centers at Brookhaven National Laboratory and the NERSC facility as useful additional locations for better redundancy and more efficient access to the data from greater number of locations.

7.2 Collecting and Storing Raw Data

7.2.1 Executive Summary

As we will show in subsequent sections, the total amount of data to be collected during the prototype operation will be considerable under all assumptions and estimates. To fulfill the mission of this test beam experiment, we expect that we will need tape storage of $O(PB)$ size, and a more modest disk space for raw data staging at CERN, for replication purposes. There will be additional requirements for processed and Monte Carlo data placement which we expect to be mostly done in the US (but not exclusively).

7.2.2 Event Size Estimates

In addition to the principal sensitive volume where Liquid Argon will serve as active medium, the prototype will also contain a Photon Detector designed to record light pulses produced in Argon due to scintillation caused by ionizing radiation. In any realistic scenario, the amount of data to be produced by the Photon Detector will be quite small compared to that of the Liquid Argon TPC. Same goes for other elements of the experimental apparatus (hodoscopes, trigger systems etc) and as a result, for the purposes of this section, we will focus only on the Liquid Argon TPC as the critical and massive source of data.

At the time of writing, work is being done on determination of the physical design of the Liquid Argon prototype, and the number of the Anode Plane Assemblies (APA) to be included in the detector is not yet finalized (e.g. 3 vs 6). There is therefore at least a factor of two uncertainty in the number of readout channels in the detector (e.g. 7680 vs 15360). This would affect the amount of data produced by DAQ (although not necessarily by a factor of two since a large part of the raw data will be zero-suppressed and occupancy in general is expected to be low), and there will be additional tracks (or track segments) produced by cosmic ray muons. From the two channel count numbers quoted above, we assume the smaller number of channels for the purposes of this discussion.

Some estimates for the scale of the data representing a charged track in the 0.5-10.0 GeV range (which is characteristic of the CERN test being planned) can be made based on existing earlier calculations for the beam neutrino events as they would appear in the LBNE Far Detector. For this we assume digitization rate fixed at 2MHz, and 4312 samples per drift window. The theoretical upper limit on the number of channels above the threshold of zero-suppression will be approximately of the order of channel count in a single APA, i.e. around 2500. Since each sample is 16 bit (12 bit is the more recent number), we arrive to the limit of approximately 20MB per single charged track. For this class of events, the amount of data will scale roughly linearly with the length of the track (cf. cases when a track is stopped or leaves the sensitive volume).

In most cases the data will be zero-suppressed at the source. The data reduction factor will depend on a variety of parameters, but as a rule of thumb it's an order of magnitude. We conclude therefore that we will have events of typical size of a few megabyte. We present quantitative estimates in 7.2.4.

7.2.3 “Before” and “After” Readout Windows

According to various estimates, given the volume of the LAr prototype, we can expect $O(1)$ cosmic ray tracks to overlay the triggered “beam” events. This leads to extra data included in each event by a value commensurate with single muons.

In addition to increasing the size of each nominal beam event, there is another consequence of this type of background. Since one of the principal goals of this experiment is to create a data sample which will allow us to precisely characterize and improve tracking and pattern recognition algorithms of a realistic detector, there must be ways to distinguish signals due to the incident beam particle vs various sources of background, of which most important is the cosmic ray background. Since overlay of cosmic ray muons over beam events is stochastic in nature, we need to make an effort to record those signals which were produced “just before” and “just after” the arrival of the test particle from the beamline, and thus be able to account for partial background tracks in the main event, with a high degree of certainty. Since the natural time scale of the detector is the total drift time for the collection volume, this leads to the requirement that we record three time windows instead of one. For the purposes of the data volume bookkeeping, this translated into adding three muon tracks worth of data, to the nominal event.

7.2.4 Statistics and the Volume of Data

Experimental program for the test includes triggering on a few types of particles over a range of momenta. We introduce bins for the particle momenta as shown in the table below. The estimated event sizes listed in the table

are based on Monte Carlo studies performed earlier for the 10kt version of the LBNE Far Detector. Hadronic and electromagnetic showers were included in these estimates. As a concrete example, for an incident electron of 4GeV/c momentum calculations indicate an average event size of \sim 2MB, after zero-suppression.

| Particle Type | Momentum Range (GeV/c) | Bin (MeV/c) | Approx. event size, MB | Approx. # of events, 10^6 |
|-----------------|------------------------|-------------|------------------------|-----------------------------|
| p | 0.1-2.0 | 100 | 1 | 1 |
| p | 2.0-10.0 | 200 | 5 | 1 |
| μ^\pm | 0.1-1.0 | 50 | 1 | 1 |
| μ^\pm | 1.0-10.0 | 200 | 5 | 1 |
| e^\pm | 0.1-2.0 | 100 | 1 | 1 |
| e^\pm | 2.0-10.0 | 200 | 4 | 1 |
| K^+ | 0.1-1.0 | 100 | 1 | 1 |
| $\gamma(\pi^0)$ | 0.1-2.0 | 100 | 1 | 1 |
| $\gamma(\pi^0)$ | 2.0-5.0 | 200 | 5 | 1 |

Preliminary plans call for statistics of the order of $10^5 - 10^6$ events to be collected in each bin, so in the table above we marked it as nominal 1M events for each entry. The requirements to the scale of these statistics are currently being refined.

Depending on the assumptions, this translates into \sim 220 million events total (for all event classes) to ensure enough statistics for subsequent analysis. Utilizing a spreadsheet model, and taking into account the cosmic ray overlay and additional readout windows as explained in 7.2.3, we arrive to a number of \sim 3PB for total storage space necessary to host the raw data. This needs to be looked at as the basis for tape budget. As explained below, this volume of data needs to be replicated for assured preservation, in at least one more additional facility, hence in effect this number must be doubled when budgeting tape.

7.2.5 Data Acquisition and Storage

The Data Acquisition System used in this experiment will be derived from the system currently used in the 35t Liquid Argon prototype being commissioned at FNAL. We foresee three Linux workstations equipped with interface cards to be used for data readout. It will be necessary to provide a stage-out disk space (a few tens of TB in size) to serve as a buffer for the DAQ system, from which the data will be transmitted to

- Tape storage at CERN.
- Storage facility at Fermilab, where the data will be written to tape and also staged in dCache as necessary for express analysis.
- *Optional* other locations, such as auxiliary storage at Brookhaven National Laboratory , which is now being planned according to the data

volumes estimated in this paper. NERSC facility has considerable potential in serving as an additional data hub. Partial copies will be transmitted to other National Laboratories and research centers.

Considerable volume of the raw data makes unlikely that it will be all staged on disk at any single location, in its entirety. We foresee the need for ample amount of tape storage, and a smaller disk space (\sim 0.5-1.0PB) for staging raw data coming out of the detector - in transit to tape storage and CERN and the US facilities.

7.2.6 Raw Data Transmission and Distribution

As mentioned in 7.2.5, at least two full replicas will exist for the raw data - at CERN and at FNAL (and likely an additional replica at BNL). Moving data outside CERN is subject to a number of requirements that include:

- automation
- monitoring
- error checking and recovery (redundant checks to ensure the “precious” data was successfully sunk to mass storage at the endpoint)
- compatibility with lower-level protocols that are widespread, well understood and maintained (cf. gridFTP)

There are a number of systems that can satisfy these requirements, and one of them where we possess sufficient expertise and experience is Spade, first used in IceCube [?] and then enhanced and successfully utilized in Daya Bay experiment [?].

Note that at this stage of the lifecycle of the data we foresee transmission between fixed endpoints (with sufficient degree of automation, checking, redundancy etc) but we haven’t discussed yet the topic of how such data is made available to researchers who wish process it at their home institution or on the Grid/in the Cloud - this will be addressed in 7.5.

7.3 Databases

A few types of databases will be required:

- Run Log, Conditions and Slow Controls records
- Offline Calibrations

Databases listed in the former item will need to be local to the experiment in order to reduce latency, improve reliability, reduce downtime due to network outages etc. A replication mechanism will need to be put in place so the data is readily available at the US and other sites. The volume of data stored in these databases will likely to be quite modest.

As to the offline calibrations, for optimal access, such databases should be located closer to the location where most processing will take place. FNAL is a good candidate for that (also from the support point of view), and we shall also consider replication of these database to other research institutions.

7.4 A note on Simulation and Reconstruction Software

Research effort connected to the “Full Scale” prototype at CERN will benefit from utilizing simulation toolkits, and tracking and other reconstruction algorithms created by communities such as former LBNE, and especially during the 35t test at FNAL. In order to leverage this software and expertise, appropriate manpower will need to be allocated in order to create and maintain physics analysis tools necessary to fulfill the research goals of this experiment.

These tools will rely on software components which will need to be portable, well maintained and validated, given the widely distributed nature of the Collaboration and the need to use geographically dispersed resources. To ensure that this happens, we plan to establish close cooperation among participating laboratories and other research institutions. The software will also need to be amenable to running on Grid facilities, and will require Distributed Data capability (see 7.5).

7.5 Distributed Computing, Workload and Workflow Management

7.5.1 Scale of the Processed Data

According to our estimates, the volume of raw data will be in the petabyte range. The offline data can be classified as follows:

- Monte Carlo data, which will contain multiple event samples to cover various event types and other conditions during the measurements with the prototype detector
- Data derived from Monte Carlo events, and produced with a variety of tracking and pattern recognition algorithms in order to create a basis for the detector characterization
- Intermediate calibration files, derived from calibration data
- Processed experimental data, which will likely exist in a few branches corresponding to a few reconstruction algorithms being applied, with the purpose of their evaluation

In the latter, there will likely be more than one processing step, thus multiplying data volume. There is sometimes a question about how much of the raw data should be preserved in the processed data streams. Given a relatively large volume of raw data, the answer in this case will likely

be “none” - for practical reasons, meaning that the derived data will be just that, and that the size of the processed data will likely be significantly smaller than the input (the raw data). Given consideration presented above, we will plan for \sim 1PB of tape storage to keep the processed data. For efficient processing, disk storage will be necessary to stage a considerable portion of both raw data (inputs) and one or a few steps in processing (outputs).

Extrapolating from our previous experience running Monte Carlo for the former LBNE Far Detector, we estimate that we’ll need a few hundred TB of continuously available disk space. In summary, we request 2PB of disk storage at FNAL to ensure optimal data availability and processing efficiency. Access to distributed data is discussed below.

7.5.2 Distributed Data

We foresee that data analysis (both experimental data and Monte Carlo) will be performed by collaborators residing in many institutions and geographically dispersed. In our estimated above, we mostly outlined storage space requirements for major data centers like CERN and FNAL. When it comes to making these data available to the researchers, we will utilize a combination of the following:

- Managed replication of data in bulk, performed with tools like Spade discussed above. Copies will be made according to wishes and capabilities of participating institutions.
- Network-centric federated storage, based on XRootD. This allows for agile, just-in-time delivery of data to worker nodes and workstations over the network. This technology has been evolving rapidly in the past few years, and solutions have been found to mitigate performance penalty due to remote data access, by implementing caching and other techniques.

In order to act on the latter item, we plan to implement a global XRootD redirector, which will make it possible to transparently access data from anywhere. A concrete technical feature of storage at FNAL is that there is a dCache network running at this facility, with substantial capacity which can be leveraged for the needs of the CERN prototype analysis. This dCache instance is equipped with a XRootD “door” which makes it accessible to outside world, subject to proper configuration, authentication and authorization.

As already mentioned, we plan to host copies of a significant portion of raw and derived data at Brookhaven National Laboratory, where substantial expertise exists in the field of data handling and processing at scale, due to the principal role this Laboratory plays in both RHIC (e.g. STAR) and ATLAS experiments. Initial simple tests of XRootD federation to access data residing at FNAL, from a XRootD instance located at BNL have been successful. At this point in time we are formulating the hardware requirements

that need to be fulfilled in order for BNL to play the role of an additional data center as described here.

7.5.3 Distributed Processing

At the time of writing, FNAL provides the bulk of computational power for LBNE (not to mention a few other IF experiments), via Fermigrid and other facilities. We plan to leverage these resources to process the prototype data. At the same time, we envisage a more distributed computing model where Grid resources are available transparently and sometimes on the opportunistic basis, using facilities made available by national Grids and in the case of the United States, by the Open Science Grid Consortium.

There are currently very large uncertainties regarding what scale of CPU power will be required to process the data, given that tracking, reconstruction and other algorithms are in a fairly early stage of development. The best estimates we have at this point range from 10 to 100 seconds required by a typical CPU to reconstruct a single event. This means that utilizing a few thousand cores through Grid facilities, it will be possible to ensure timely processing of these data.

We have not chosen yet the type of Workload Management System to be used for the purposes of the CERN prototype test. Currently, many researchers at FNAL are using the *jobsub* tool, which opens access to Fermigrid and additionally to the Open Science Grid and Cloud resources. There are other capable (and arguably more sophisticated) system being used, for example by the LHC experiments. We plan to conduct an evaluation of these systems with a view to adopt a different solution if necessary.

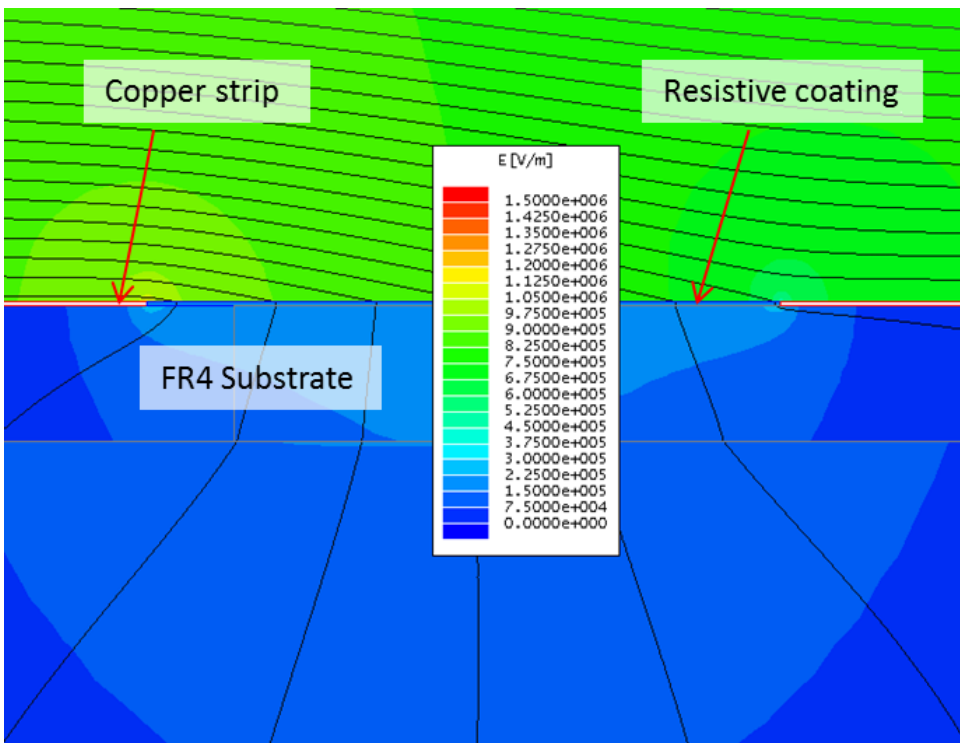


Figure 12: Plot of electric field (color contours) and equi-potential contours (black lines) in a small region around the edges of two adjacent field cage strips on a 1.6mm thick FR4 substrate. A layer of resistive coating between the two copper strips nearly eliminated the high electric field regions at the copper edges.

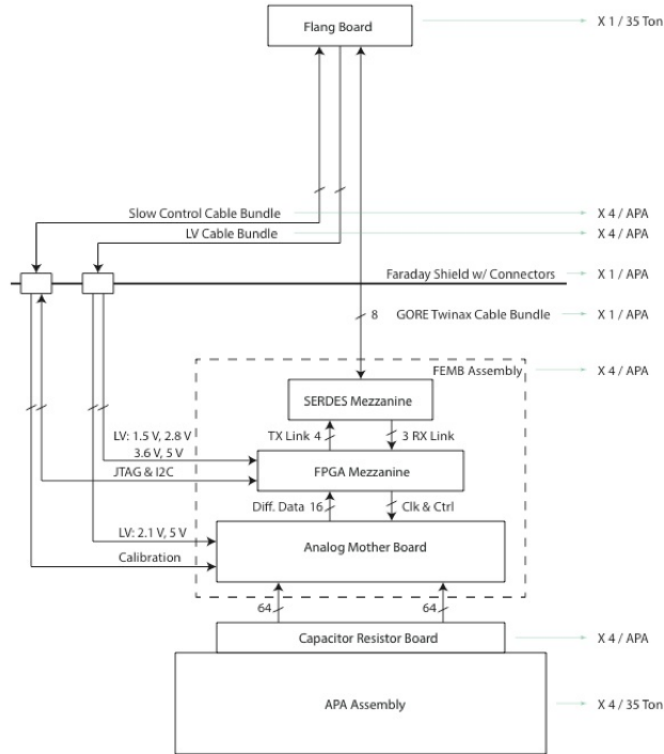


Figure 13: Schematic for the TPC cold FE electronics. ***MG*** Not sure if this is high enough quality. ***Ask Chen for source and fix numbers.

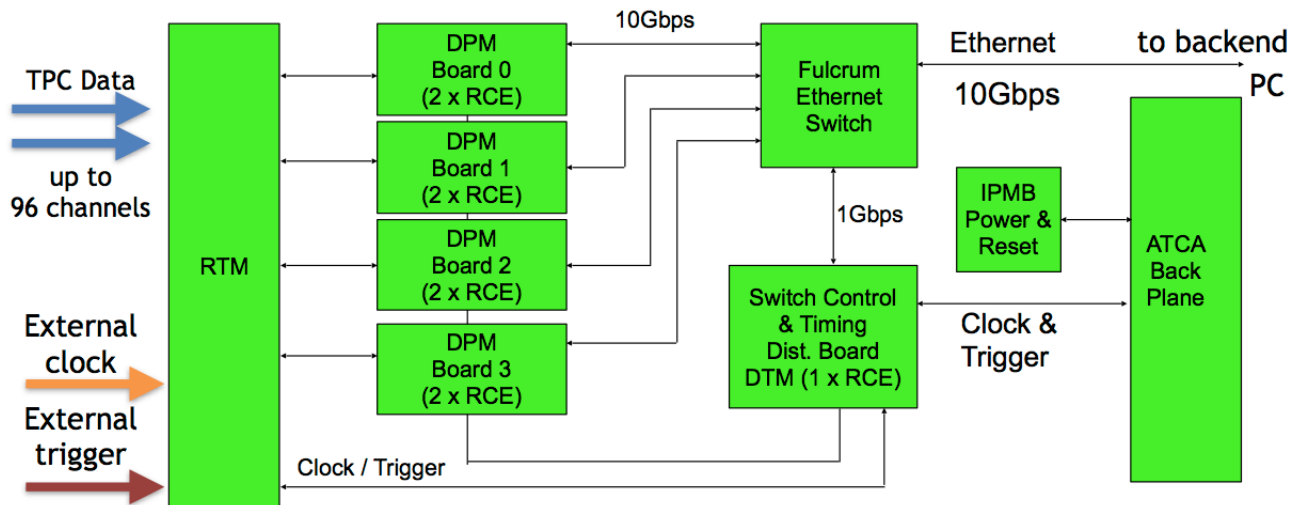


Figure 14: Schematic for the TPC DAQ system.

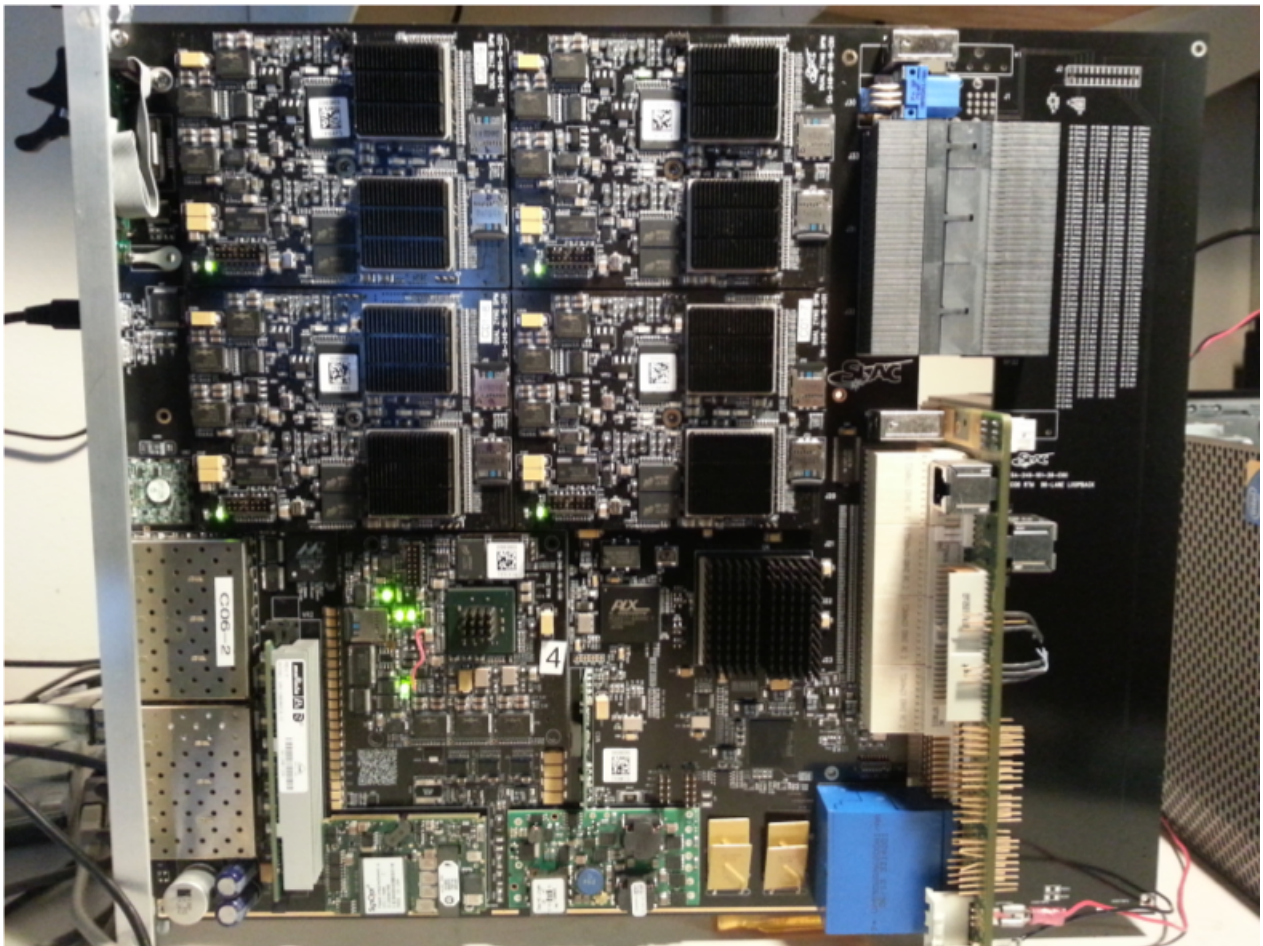


Figure 15: The COB (left of the large connectors) and RTM (right).

GST® Containment System

AS A PRIMARY BARRIER :

a flexible (1.2mm) stainless steel membrane



The double network of corrugations absorbs the thermal contractions due to the very low temperature of the LNG.

Insulating panel

The thickness of the panels can be adjusted to provide a large range of boil-off rates according to the operator's requirements (typically 0.05% per day).

Plywood

Reinforced polyurethane foam

AS A SECONDARY BARRIER :

a composite laminated material

This consists of a thin sheet of aluminium between two layers of glass cloth and resin.

In the event of a failure of the primary membrane, it prevents the build-up of stress concentrations on concrete corner and ensures the liquid tightness of the concrete wall.

Reinforced polyurethane foam

Plywood

Mastic

Post-tensionned concrete covered by a moisture barrier

The outer concrete container provides the *structural resistance* to internal (LNG hydrostatic & dynamic pressure, and vapour gas pressure) and external (wind, snow, ice) loads.

A moisture barrier, applied on its inner side, prevents moisture from entering the tank.

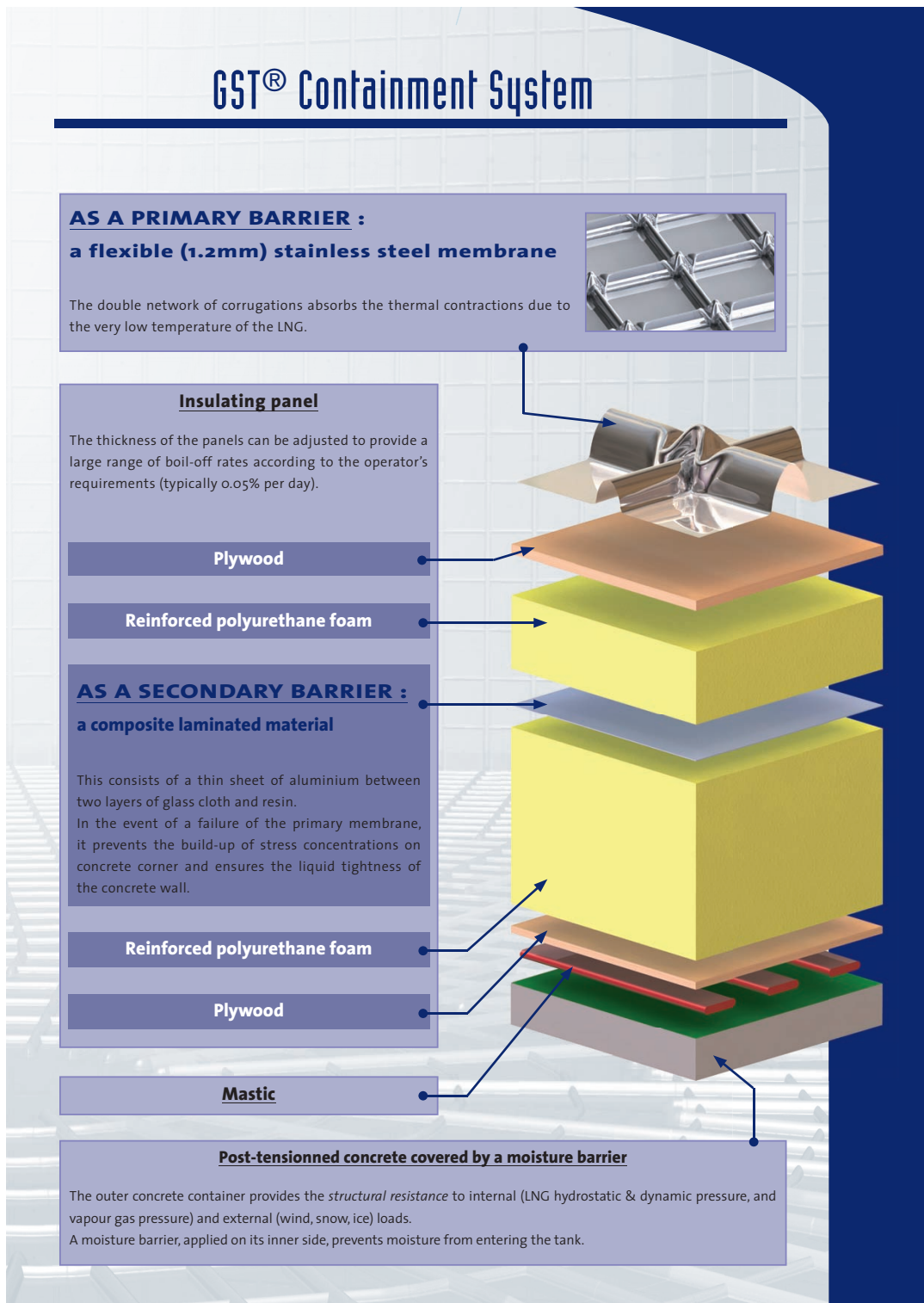


Figure 16: Exploded view of the membrane cryostat technology

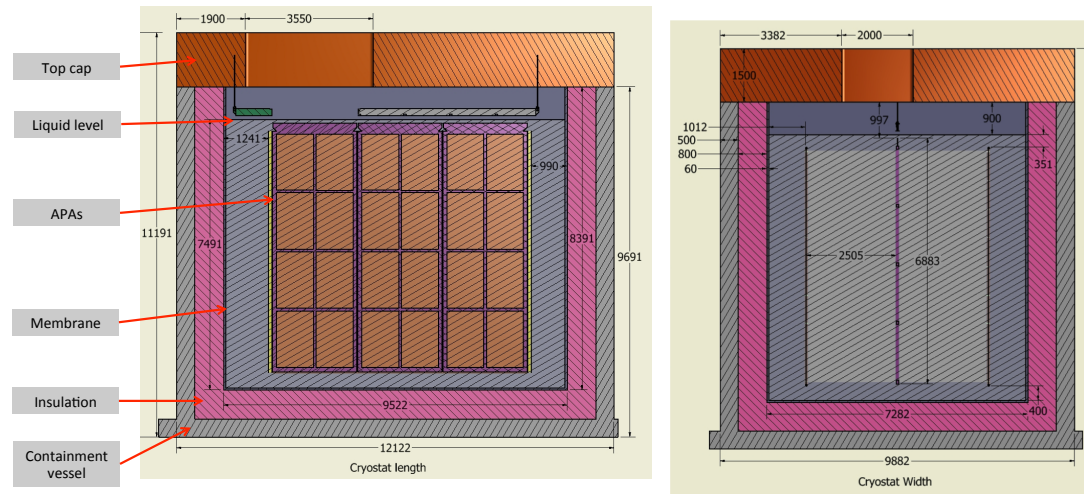


Figure 17: Side (left) and end (right) views of cryostat

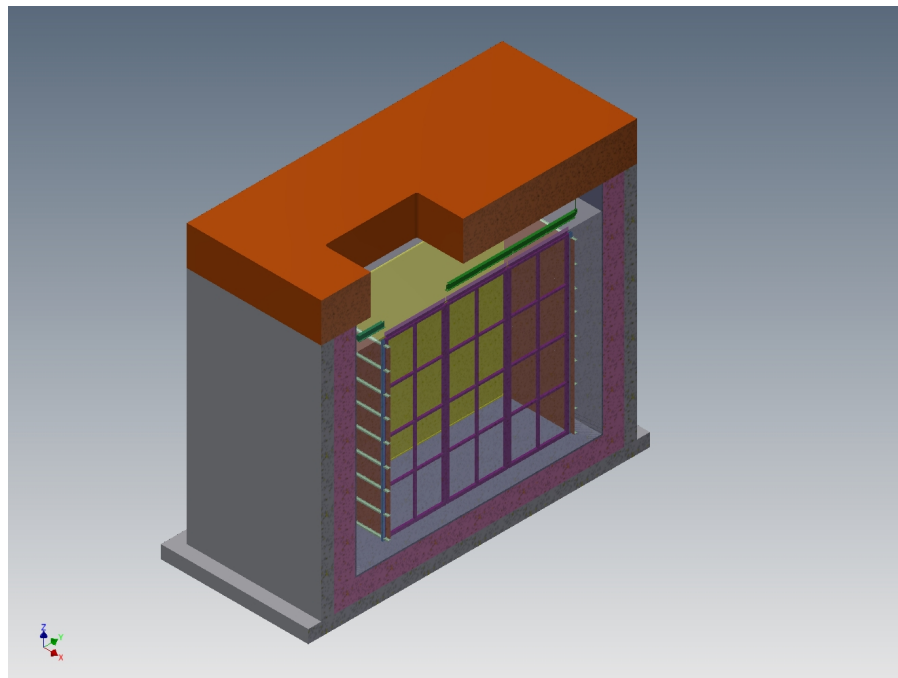


Figure 18: Isometric view of the membrane cryostat

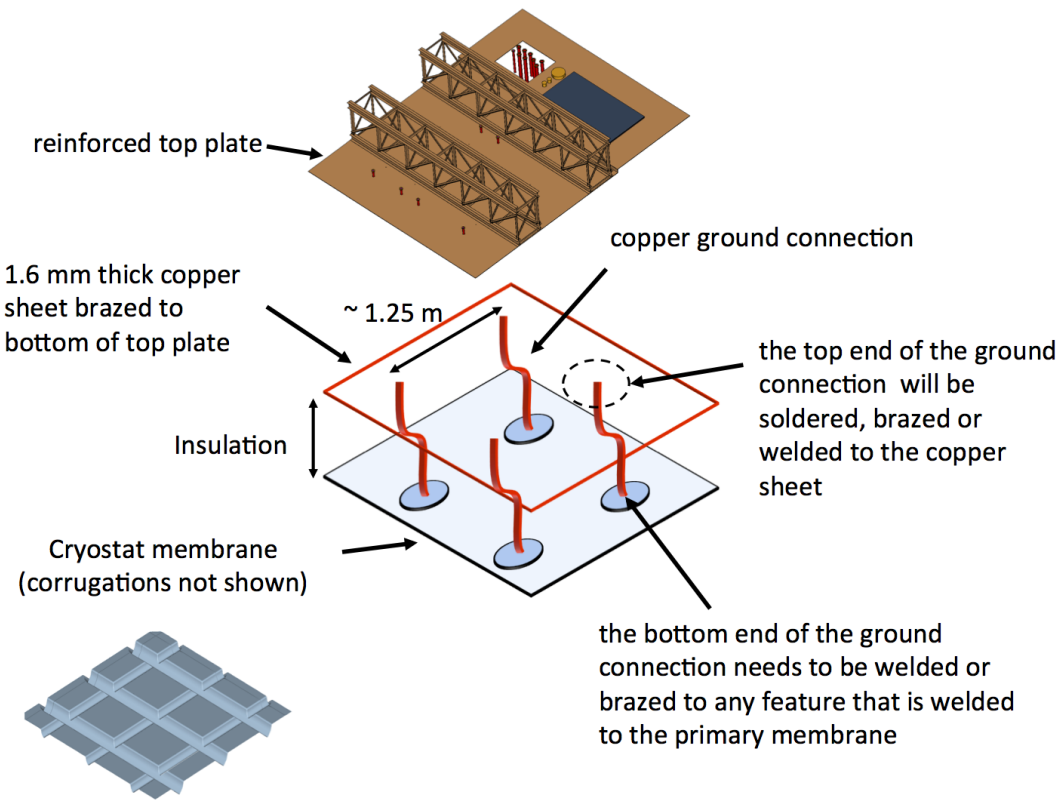


Figure 19: Top plate grounding layout

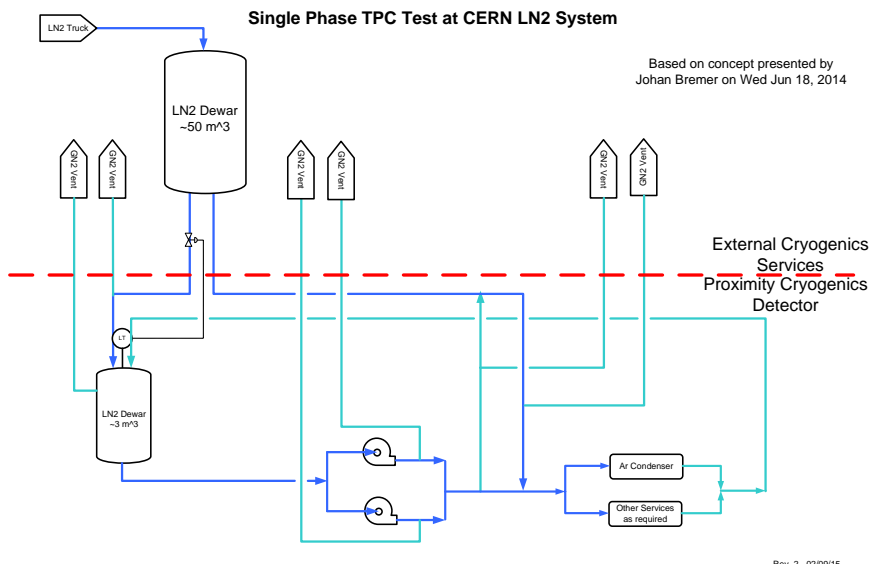


Figure 20: Schematic diagram for the proposed LN2 system

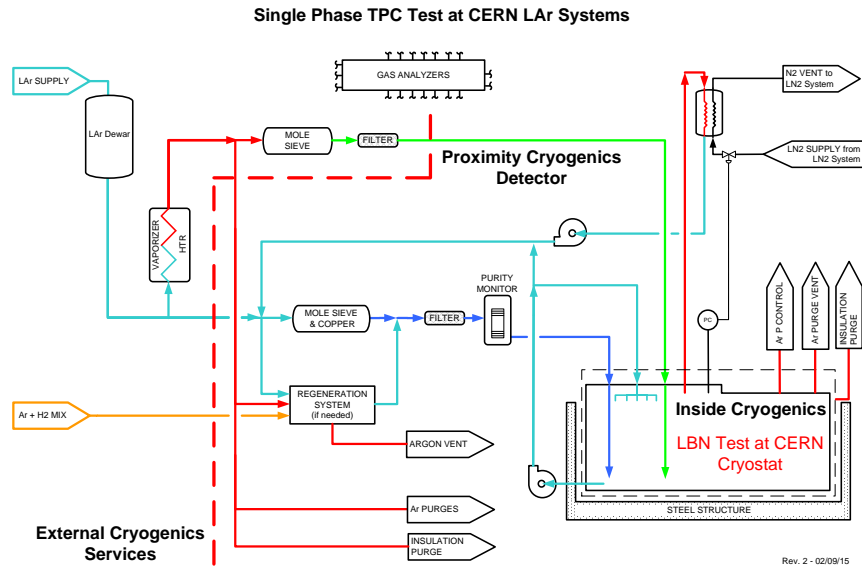


Figure 21: Schematic diagram for the proposed LAr system

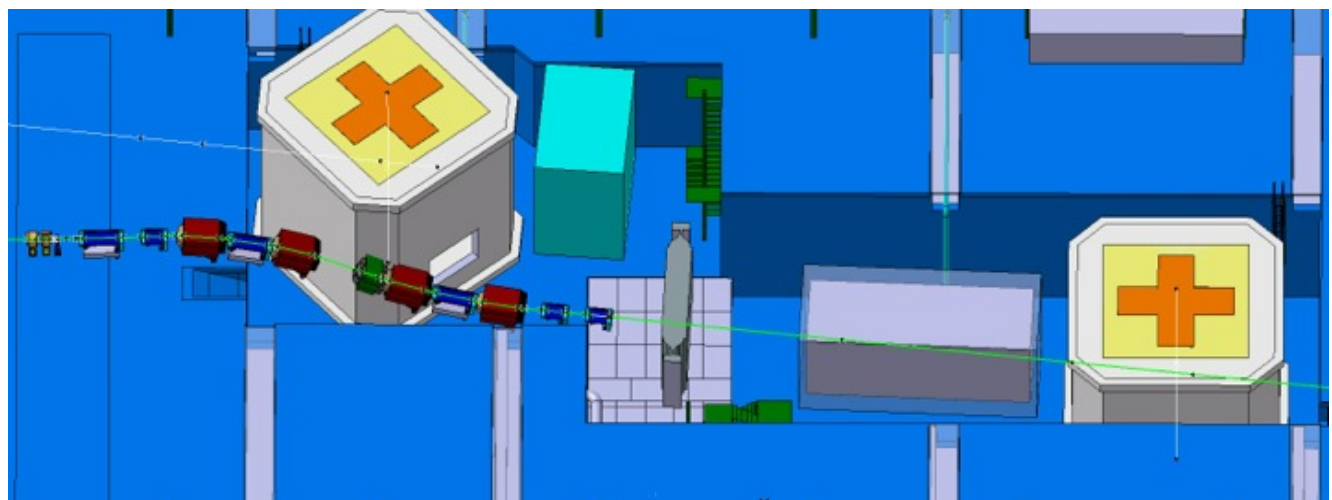


Figure 22: Preliminary layout of the H4ext beamline